

# Bayesian sequential data assimilation for COVID-19 forecasting

Maria L. Daza-Torres <sup>\*1,3</sup>, Marcos A. Capistrán<sup>1</sup>, Antonio Capella<sup>2</sup>, and J. Andrés Christen<sup>1</sup>

<sup>1</sup>*Centro de Investigación en Matemáticas, CIMAT, Guanajuato, Mexico*

<sup>2</sup>*Instituto de Matemáticas, UNAM, Circuito Exterior, CU, CDMX, Mexico*

<sup>3</sup>*Department of Public Health Sciences, University of California Davis, California, United States*

May 31, 2021

## Abstract

We introduce a Bayesian sequential data assimilation and forecasting method for non-autonomous dynamical systems. We applied this method to the current COVID-19 pandemic. It is assumed that suitable transmission, epidemic and observation models are available and previously validated. The transmission and epidemic models are coded into a dynamical system. The observation model depends on the dynamical system state variables and parameters, and is cast as a likelihood function. The forecast is sequentially updated over a sliding window of epidemic records as new data becomes available. Prior distributions for the state variables at the new forecasting time are assembled using the dynamical system, calibrated for the previous forecast. Epidemic outbreaks are non-autonomous dynamical systems depending on human behavior, viral evolution and climate, among other factors, rendering it impossible to make reliable long-term epidemic forecasts. We show our forecasting method's performance using a SEIR type model and COVID-19 data from several Mexican localities. Moreover, we derive further insights into the COVID-19 pandemic from our model predictions. The rationale of our approach is that sequential data assimilation is an adequate compromise between data fitting and dynamical system prediction.

**Keywords**— Bayesian inference, data assimilation, COVID-19, SEIRD.

## 1 Introduction

The current COVID-19 pandemic is a major challenge to the world population. Reliable model-based forecasts are required to assist healthcare authorities in decision-making and planning. Compartmental epidemic models have proven to be adequate to assimilate epidemic data and making forecasts [1, 2]. However, epidemic dynamics is a non-autonomous dynamical system in which model parameters, e.g. contact rates, evolve in time. Indeed, epidemic outbreak predictability is

---

<sup>\*</sup>E-mail: mdazatorres@cimat.mx; mdazatorres@ucdavis.edu

limited due to the influence of human behavior, incomplete knowledge of the virus's evolution, and weather [3, 4], as well as delay and under-reporting of new cases and deaths [5, 6], and the size of the initial susceptible population.

For a non-autonomous dynamical system inference problem, we may introduce time-dependent parameters for the entire evolution and try to fit their values for all times [7]. However, the complexity of the resulting inference increases with the amount of data and may make the inference process infeasible. Moreover, fitting the whole of the epidemic to infer initial state values for an epidemic lasting several months ceases to be useful. For instance, in [7] only the contact rate varies with time, and the resulting MCMC is cumbersome and challenging to run. In fact, given the generation interval of COVID-19, data beyond one month in the past should start to have less importance for nowcasting and predictions. A practical compromise is to make probabilistic epidemic forecasts a few weeks ahead in a moving window [8, 9] and recalibrate regularly. Consequently, all model parameters evolve in time, and the inference problem splits into smaller ones. In this approach, the method should account explicitly for data delay and under-reporting.

In this paper, we introduce a Bayesian sequential data assimilation and forecasting method for non-autonomous dynamical systems. We applied this method to the current COVID-19 pandemic. We assume that transmission, epidemic, and observation models are properly postulated and previously validated. The transmission and epidemic models are coded into a dynamical system following the mathematical epidemiology theory [10, 11]. In this case, we postulate a SEIR type epidemic model with Erlang [12] residence times in the exposed and infected compartments to model non-exponential residence times. The observation model, cast as a likelihood function, depends on the dynamical system state variables and parameters [13]. We elicit prior distributions on the susceptible population size, the dynamical system initial conditions, and the infectious contact rates. With a Markov Chain Monte Carlo we infer parameters and predict quantities of interest (QoI), such as hospital occupancy in a metropolitan area during the epidemic outbreak. The inference begins when the community transmission starts, and we infer parameters and predict QoI for a couple of weeks into the future. As new data becomes available, we update the forecast sequentially over a sliding window in time. New prior models are defined from the current parameters and state variables posterior distributions. New posterior distributions are computed within each new window beyond the available epidemic records to produce the forecasts. Moreover, we constrain changes in the contact rate and susceptible population size naturally through auto-regressive models on the corresponding parameters. We argue that this is a natural approach to data assimilation and forecasting with an epidemic. To sustain this claim, we show our forecasting method's performance using a SEIR type model and COVID-19 data from several Mexican localities.

## 1.1 Related work

Real time epidemic forecasting is an emerging research field [14]. Many forecast modeling efforts study how to address data under-reporting and delays [9, 15]. Other efforts are directed at exploring what sources of information can be incorporated as covariates to make better forecasts. McGough *et al.* [16] incorporate traditional surveillance with social media data to forecast Zika in Latin America. The RAPIDD ebola forecasting challenge [17] explored how to integrate different sources of data for Ebola forecasting. Hii *et al.* [18] use temperature and rainfall to forecast dengue incidence.

In a related work, [7] present a COVID-19 prediction model. Using a SEIR type dynamical model, and including hospital dynamics and Erlang compartments [12] to properly model residence times, [7] model and predict the COVID-19 epidemic in the Mexican 32 states and several metropolitan areas, from the epidemic onset in Mexico in March 2020 (and until February 2021, see <https://coronavirus.conacyt.mx/proyectos/ama.html>, in Spanish; model *ama2*).

## 1.2 Contributions and limitations

The probabilistic forecasting method introduced in this paper allows to reliably predict the incidence of new cases and deaths one to four weeks ahead of time. Once we are near or after a local incidence maximum, our forecasting method disentangles the role of infectious contact rate and effective population size. Other quantities of interest such as hospital occupancy can be calculated as a byproduct of the forecast using suitable renewal equations.

More general data analysis, e.g. by age groups, is not presented in this work. However, our results may be applicable on those cases, provided suitable transmission and epidemic models are available. The estimation of the time varying effective population size obtained in this paper has a large variance, provided we use a mean field equations to represent the underlying epidemics' dynamics, which is a stochastic process on a network. Finally, it is not straightforward to compute the accumulated number of cases nor the accumulated number of deaths using our approach.

This manuscript is organized as follows. In Section 2 we make a summary of the modeling decisions taken to implement our forecasting method. In Section 3 we apply our method to COVID-19 epidemic data. Finally, in Section 4 we present the analysis of the Mexico City data. Other examples are provided in the Supplementary material (SM).

## 2 Bayesian Sequential Forecasting Method

Let us assume that community transmission starts at time  $t = t_0 - L - D$  at the metropolitan area where the outbreak is being analyzed. Set  $k = 0$  and denote by  $[t_k - L - D, t_k - D]$  the learning period. Namely, the period when we collect epidemic records  $z^{(k)}$  to create a forecast. In the example presented in Section 3, these epidemic records are new hospital admittances and deaths. The delay period is  $[t_k - D, t_k]$ , i.e. the period when epidemic records are not mature and may include delays in reporting. The forecasting day, from which forecasting starts, is  $t_k$ . We refer to  $[t_k, t_k + F]$  as the forecasting period, and  $[t_k - L - D, t_k + F]$  is the forecasting window as illustrated in Figure 2.

Let  $x(t) = (S(t), E(t), I(t), \dots)^T$  denote the time-dependent vector of state variables. We shall assume that the epidemic and transmission models are posed as an initial value problem for a nonlinear system of ordinary differential equations

$$\begin{aligned} \dot{x}(t) &= f(x(t), \theta_k) \\ x(t_k - L - D) &= x_k, \end{aligned} \tag{1}$$

where  $t_k - L - D$  and  $x_k$  denote respectively the initial time and state in the forecasting window  $[t_k - L - D, t_k + F]$ , and  $\theta_k$  is a vector of model parameters (e.g. contact rate  $\beta$ , effective population size  $\omega$ , etc.) used to calibrate model (1). We shall denote  $p^{(k)} = (x_k, \theta_k)$  the joint vector of initial conditions and model parameters to be inferred, and  $x(t, p^{(k)})$  is the solution of problem (1) at time  $t$  with parameters  $p^{(k)}$ . Note that, from the onset,  $p^{(k)}$  is assumed to be changing in time with each forecast window  $k$ .

If  $k = 0$ , we postulate a prior distribution  $\pi_{P^{(k)}}(p^{(k)})$ , a likelihood  $\pi_{Z^{(k)}|P^{(k)}}(z^{(k)}|p^{(k)})$  and use equation (1) and samples obtained through Markov Chain Monte Carlo of the corresponding posterior distribution  $\pi_{P^{(k)}|Z^{(k)}}(p^{(k)}|z^{(k)})$  to make a probabilistic prediction of  $x(t)$  in the forecasting period  $t \in [t_k - L - D, t_k + F]$ . Afterwards, we update the forecasting window by setting  $t_{k+1} = t_k + n$ , where  $n$  is the number of days until the next forecast (commonly, weekly updates  $n = 7$  are performed). We assemble a new prior distribution  $\pi_{P^{(k+1)}}(p^{(k+1)})$  for the model parameters  $p^{k+1}$  in the new forecasting window  $[t_{k+1} - L - D, t_{k+1} + F]$  using the predicted values of  $x(t)$  at  $t = t_{k+1} - L - D$  obtained with equation (1) and samples of the posterior distribution  $\pi_{P^{(k)}|Z^{(k)}}(p^{(k)}|z^{(k)})$

of the previous forecast. Model parameters  $\theta_{k+1}$  have an autoregressive prior distribution in terms of  $\theta_k$ . Finally, we set  $k \leftarrow k + 1$  and repeat the above process to create a new forecast. In passing, note that this fits correctly with the inherent sequential nature of Bayesian inference in which “today’s posterior is tomorrow’s prior” (D. Lindley, [19], p. 2).

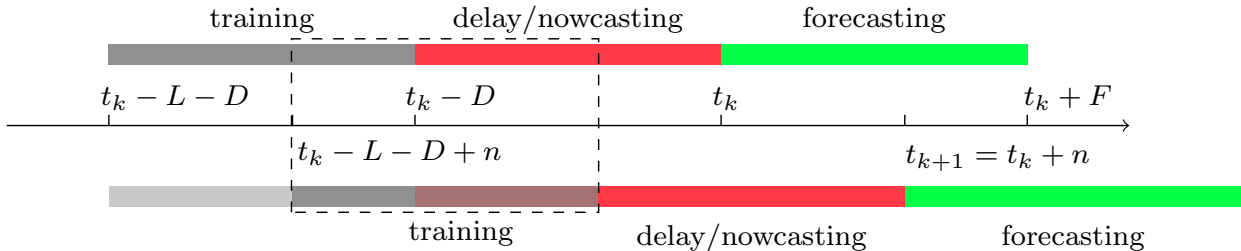


**Figure 1: Bayesian Sequential data assimilation.** We propose a Bayesian filtering method that predicts along the dynamical system (1). The model is fitted with data in the training period and this is used to make predictions during the reporting delay period (nowcasting) and a forecasting period. The training window is updated and moved  $n$  days forward, to update all forecasts and the former posterior becomes the prior, in the next window. Further details are described in Algorithm 1.

The Bayesian sequential data assimilation method consists of three parts; a dynamical system that codes the transmission and epidemiological models, a probabilistic model for the observed incident cases and deaths, and an informed prior distribution for the parameter space in each forecasting period. In Section 3, we show how to postulate each model component for a forecasting model of COVID-19 using data from several Mexico localities.

### 3 Example: A SEIR type model

#### 3.1 Dynamical model

We consider a variation on the SEIRD epidemic model for susceptible, exposed, infectious, removed, and dead individuals. We have added a compartment for unobserved infectious individuals.

We assume that the total population of the metropolitan area being analyzed is  $N$ . We assume further that there is only a few infected individuals at the onset of community transmission. Susceptible individuals  $S$  become exposed  $E$  with force of infection  $\lambda$ . The transmission model is coded into  $\lambda$  as follows. We assume that only unobserved ( $U$ ) and observed ( $O$ ) infectious individuals spread the infection, that is

$$\lambda = \frac{(U + \kappa O)\beta}{\omega \cdot N},$$

where  $\beta$  is the infectious contact rate and  $\omega$  is the proportion of effective population size during the outbreak. We have assumed that the contact rate for observed infectious is a factor ( $\kappa$ ) of the contact rate for unobserved infectious. A fraction  $f$  of exposed individuals proceeds to the observed infected class ( $O$ ) at rate  $\sigma_1$ , while the remainder goes directly to an unobserved ineffective stage ( $U$ ), also at rate  $\sigma_1$ . Individuals leave the infectious class at rate  $\sigma_2$ , with a fraction  $1 - g$  recovering and going to the removed class ( $R$ ) and the remainder ( $g$ ) dying of infection. Unobserved individuals go to the removed stage at rate  $\gamma$ . We split the  $E$ ,  $I$ , and  $O$  compartments into two sub-compartments to model residence rates explicitly as Erlang distributions [12], see Table 1.

---

**Algorithm 1:** Bayesian sequential data assimilation for COVID-19 forecasting

---

Input. Length in days of the learning ( $L$ ), delay ( $D$ ) and forecast ( $F$ ) periods. A prior distribution for parameters and initial conditions at the onset,  $k = 0$ . Outbreak initial time  $t_0 - L - D$ . Data ( $z^{(k)}$ ) for  $k = 0, 1, \dots$  forecasting windows.

Output. 

- Posterior distribution  $\pi_{P^{(k)}|Z^{(k)}}(p^{(k)}|z^{(k)})$  for  $k = 0, 1, \dots$
- Prediction of QoI, e.g. hospital occupancy, report of new cases, etc, in the forecasting period  $[t_k, t_k + F]$  for  $k = 0, 1, \dots$  forecasting windows.

Step 1. If  $k = 0$ :

Postulate the prior distribution  $\pi_{P^{(k)}}(p^{(k)})$  for parameters and initial conditions  $p^{(k)} = (x_k, \theta_k)$  at the beginning of the inference.

If  $k > 0$ :

Fit the prior distribution  $\pi_{P^{(k)}}(p^{(k)})$  for parameters and initial conditions  $p^{(k)} = (x_k, \theta_k)$  using the MCMC output from period  $k - 1$  as follows.

- (a) For the initial value of the state variables  $x(t_k - L - D) = x_k$  in the forecasting window  $[t_k - L - D, t_k + F]$ , use the MCMC output of  $p^{(k-1)}$  to fit the predictions  $x(t_k - L - D; p^{(k-1)})$  to a known distribution  $\pi_{X_k}(x_k)$  to be used as prior for  $x_k$ .
- (b) For the model parameters  $\theta_k$ , the MCMC output of  $\theta_{k-1}$  is fitted to a known distribution to be used as prior distribution  $\pi_{\Theta_k}(\theta_k)$  of  $\theta_k$ .
- (c) Set the prior distribution  $\pi_{P^{(k)}}(p^{(k)}) = \pi_{X_k}(x_k) \times \pi_{\Theta_k}(\theta_k)$

(Exact details on how these priors are adjusted from the previous MCMC sample need to be decided depending on each application, see Section 3.5.)

Step 2. Compute samples of the posterior distribution  $\pi_{Z^{(k)}|P^{(k)}}(z^{(k)}|p^{(k)})$  using MCMC.

Step 3. Use the dynamical system prediction  $x(t, p^{(k)})$  to forecast QoI up to time  $t = t_k + F$  using the MCMC posterior samples.

Step 4. Save the MCMC output for the next forecasting time.

---

The dynamics of the epidemic process is governed by the following nonlinear system of ordinary differential equations

$$\begin{aligned}\dot{S} &= -\lambda S \\ \dot{E} &= \lambda S - \sigma_1 E \\ \dot{O} &= f\sigma_1 E - \sigma_2 O \\ \dot{U} &= (1-f)\sigma_1 E - \gamma U \\ \dot{R} &= (1-g)\sigma_2 O + \gamma U \\ \dot{D} &= g\sigma_2 O,\end{aligned}$$

with initial conditions  $E(0) = E_0$ ,  $O(0) = O_0$ ,  $U(0) = U_0$ ,  $R_0 = R(0)$ ,  $D_0 = D(0)$ , and  $S(0) = N - E_0 - O_0 - U_0 - R_0 - D_0$ . Here  $N = S + E + O + U + R + D$ . A flow diagram for the model is shown in Figure 2.

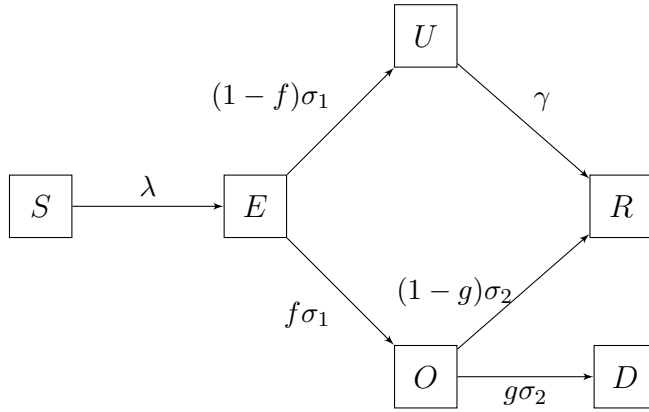


Figure 2: A SEIR type model that into account both observed and unobserved infections.

Table 1: Average times and Erlang shape parameters for sub-compartments.

Variable	Rates	Average time	Erlang shape	Reference
$S$	$\beta$	Inferred	1	
$E$	$1/\sigma_1$	5 days	2	[20, 21]
$A$	$1/\gamma$	7 days	2	[22]
$I$	$1/\sigma_2$	14 days	2	[23, 24]

In general, the components of the epidemic and contagion models, from exposition time to clinical outcome, should be posed taking into account the distribution of the residence time in each compartment, see [25] and its supplementary material. In this work, the contact rate ( $\beta$ ) pertains to the time-varying reproduction number. On the other hand, the serial interval distribution, the symptoms to death distribution, and infection to symptoms distribution are judiciously set using hospital records and references, see [7] and table 1. Finally, a proxy of the population-averaged infection fatality rate is represented through the product  $f \cdot g$ , where  $f$  is set using records of the number of infected individuals seeking help at the hospital and  $g$  is an estimated parameter that accounts for hospital fatality rate of COVID-19 patients. In this work, we infer a time-varying effective population size ( $\omega$ ), which is the fraction of the total population having contact that may lead to contagion at a given time.

Of note, once we have a reliable estimate of the residence times in the latent and infectious compartments, we can estimate and forecast hospital occupancy using suitable renewal equations. This method is flexible with respect to resident times distribution in the hospital compartments, and avoids the need of complex designs for compartments after the non-linear part of the system. For instance see [7] and the associated website of the project <https://coronavirus.conacyt.mx/proyectos/movilidad.html>.

### 3.2 Model parameters

The model has two kinds of parameters that have to be calibrated or inferred, respectively. Namely, those related to COVID-19 disease (such as residence times and proportions of individuals that split at each bifurcation of the model) and those associated with the public response to mitigation measures such as the contact rate ( $\beta$ ) and the proportion of effective population size during the outbreak ( $\omega$ ). Some of these parameters can be found in recent literature (see Table 1) or inferred

from reported cases and deaths, but some remain mostly unknown and not possible to infer from such data [7]. In the latter category, we have the fraction  $1 - f$  of unobserved infections. We assume  $1 - f = 0.2$ , which means that 80% of cases of symptomatic/asymptomatic infectious go unreported.

### 3.3 Observational model and data

The observed data used to fit the model is based on time series of incident confirmed cases and deaths. We consider daily deaths counts  $d_i$  and its theoretical expectation that is estimated in terms of the dynamical model as

$$\mu_D(t_i) = D(t_i) - D(t_{i-1}).$$

Analogously, we consider daily cases  $c_i$  and its corresponding theoretical expectation  $\mu_c(t_i)$  given by the daily flux entering the  $O$  compartment [7], namely

$$\mu_c(t_i) = \int_{t_{i-1}}^{t_i} f\sigma_1 E_2(t) dt,$$

where  $E_2(t)$  is the last state variable in the  $E$  Erlang series. We calculate the above integral using a simple trapezoidal rule with 10 points.

### 3.4 Estimating model parameters with MCMC

We consider daily confirmed cases  $c_i$  of patients with a positive test ( $O$ ) and daily reported deaths  $d_i$ , for the area being analyzed. To account for over dispersed counts, we use a negative binomial (NB) distribution  $NB(\mu, \omega, \theta)$  with mean  $\mu$  and over dispersion parameters  $\theta$  and  $\omega$  [7]. For data  $y_i$ , we let

$$y_i \sim NB(p\mu(t_i), \omega, \theta),$$

with fixed values for the over dispersion parameters  $\omega, \theta$  and the reporting probability  $p$ . We assume conditional independence in the data and therefore from the NB model we obtain a likelihood.

The parameters to be inferred are the contact rate ( $\beta$ ), the proportion of the effective population ( $\omega$ ), the fraction of infected dying ( $g$ ), and crucially we also infer the initial conditions for  $E(0)$ ,  $O(0)$ ,  $U(0)$ ,  $R(0)$ ,  $D(0)$ , letting  $S(0) = \omega \cdot N - (E(0) + O(0) + U(0) + R(0))$ . We have all initial conditions defined and the model can be solved numerically to obtain  $\mu_D$  and  $\mu_c$  to evaluate our likelihood. To sample from the posterior, we resort to MCMC using the t-walk generic sampler [26]. The MCMC runs semi-automatic, with consistent performances in most data sets.

Table 2: Parameters and prior distributions used for Bayesian inference.

Parameter	Prior distribution
Contact rate $\beta$	$LogNorm(1, 1)$
Fraction of infected dying ( $g$ )	$Beta(1 + 1/6, 1 + 1/3)$
Proportion of the effective population ( $\omega$ )	$Beta(1 + 1/6, 1 + 1/3)$

### 3.5 Bayesian filtering design

Regarding the elicitation of the parameters' prior distribution for the first forecast, at  $k = 0$ , we use Gamma distributions for the initial conditions  $E_0$ ,  $O_0$ , and  $U_0$ , with scale 1 and shape parameter 10.

This for modeling the low, near to 10, and close to zero counts for the number of initial infectious conditions. For the initial conditions  $R_0$  and  $D_0$ , we also use Gamma distributions with scale and shape parameters equal to 1. This because at the beginning of the outbreak, both parameters are close to zero. The prior distributions for the remaining parameters are summarized in Table 2. Note that, the above prior distributions are only used at the first learning window. From  $k = 1$  onwards, the MCMC posterior sample from window  $k$  is used to create a *prior* for window  $k + 1$ , as previously mentioned and explained in Algorithm 1.

Regarding how the MCMC posterior sample is used to create a prior, we proceed as follows. For each parameter, the MCMC sample mean is used to match the mean of a Gamma distribution, with over dispersion, making the standard deviation of the Gamma prior equal to 0.9 of the mean. This allows for reduced dependence on the previous period, permitting more learning in the current window. Matching all moments will signify that a single parameter (e.g.  $\omega$ ) is assumed in all windows, nonetheless a time dependent scheme was envisaged from the onset. We found this scheme to be a reasonable compromise between utilizing the previous window information and learning from the current.

Setting the lengths  $L$ ,  $D$  and  $F$  of the learning, delay and forecasting periods should be also an evidence-based modeler decision. In the example presented in this paper, we set  $L$  to twice the length from symptoms onset to mild disease clinical outcome, namely 28 days. The length of the delay period is set to 11 days, corresponding to roughly the mean of the delay in Mexican clinical laboratory reports. Finally,  $F$  is chosen to be 1,2,3 and 4 weeks.

## 4 Results

In this section, we present the results of Algorithm 1 applied to the COVID-19 pandemic for Mexico's city metropolitan area. We provide further examples of other Mexican states in the SM. The method is applied to the daily reports on the incident number of confirmed cases and deaths starting in early 2020.

We use the Bayesian Sequential Forecasting Method to predict trajectories, given weekly updates. The model starts with inaccurately predicted trajectories, where the median of the trajectories overestimate the future data (See Figure 3), and the initial prediction cones are rather wide. Early forecast uncertainty is high because we do not know yet the effective population size participating in the epidemic, namely  $\omega$  in our model. Furthermore, forecasts at this stage are prone to additional errors due to the uncertainty in disease parameters such as the transmission rate  $\beta$  and the initial state of the epidemic outbreak.

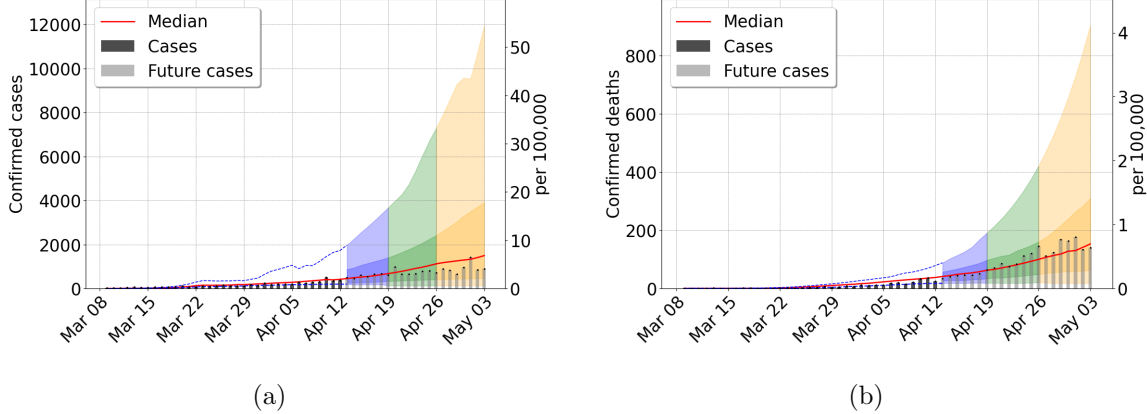
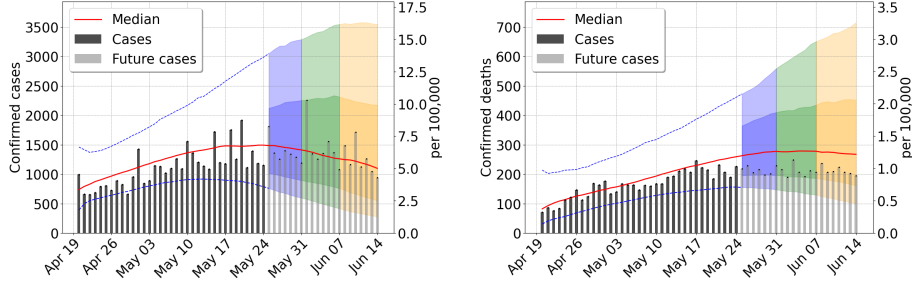


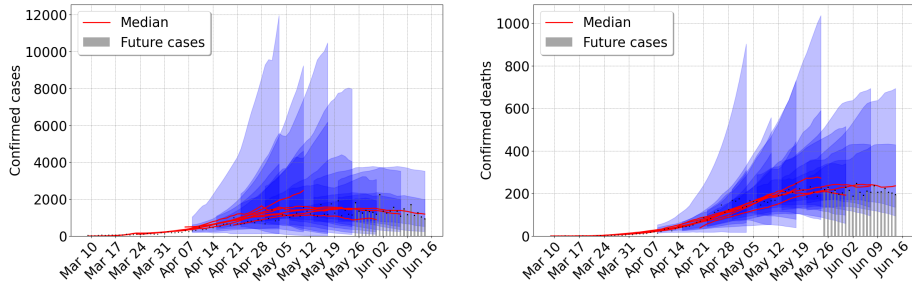
Figure 3: Forecast results for Mexico city metropolitan area, using data from March 8 to April 12, 2020. (a) Confirmed cases (b) Confirmed deaths. Central red lines indicate the median incidence forecast. The darker shaded region indicates the interquartile forecast range, and the lighter shaded region indicates the 5–95th percentile range. The colors blue, green, and orange represent the forecast 1,2, and 3 weeks ahead, respectively. Total population 21,942,666 inhabitants.

As we combine previous information with new incoming data into the next predictions, accuracy increases quickly. The median of the forecast becomes closer to future data, and the prediction cone uncertainty shrinks. In figure Figure 3 we presented the early stages of the epidemic outbreak, and in Figures 4-5 we present three later times. First, after the initial outbreak wave peak, second during late summer, where the outbreak was decreasing slowly, and third in the middle of a second intense wave in December. The results show rather uniform prediction cones during the entire evolution, increasing cone size at the onset of the second outbreak wave. Despite the larger intensity of the second wave, the prediction cones never become as large as at the early stages. We can explain this behavior by looking at the other model parameter included in our inference process.

In Figure 6, we present the weekly estimates of the infection contact rate  $\beta$ , the effective population size (or available pool of susceptible individuals)  $\omega$ , and the hospital fatality rate  $g$ . The figure shows that after an initial period where the estimates of  $\beta$  have considerable uncertainty, its median value becomes relatively stable around 0.2. At the second wave, we observe an increase in uncertainty, but  $\beta$ 's mean value remains almost constant with a slight decrease afterward. Regarding  $g$ , we also observe an initial uncertainty period, but its mean value is relatively stable, and its uncertainty becomes smaller. Finally, the effective population size behavior is somewhat different since  $\omega$  is a proxy of the complex network of people's contacts in a metropolitan area. Its estimates show a significant uncertainty for almost all times. We observe the minimum value of  $\omega$  in the early months of the pandemic with a slow increase afterward and another peak during the second wave. After the initial period, our inference method “learned” reasonable parameter values for  $\beta$  and  $g$ , and we can trace back most changes in our prediction cones to  $\omega$ . These observations explain the difference between the prediction cones between the first and second waves. Finally, we claim that changes in  $\omega$  are an accurate proxy of the population's response to mobility lockdown and release measures. To support our claim, we include in Figure 6 the plot of a mobility index derived from social media tracking, see <https://coronavirus.conacyt.mx/proyectos/movilidad.html> (In Spanish). The correlation of both quantities is unmistakable. In the SM, we present our estimates for all 32 Mexican states where almost all the above analysis apply.

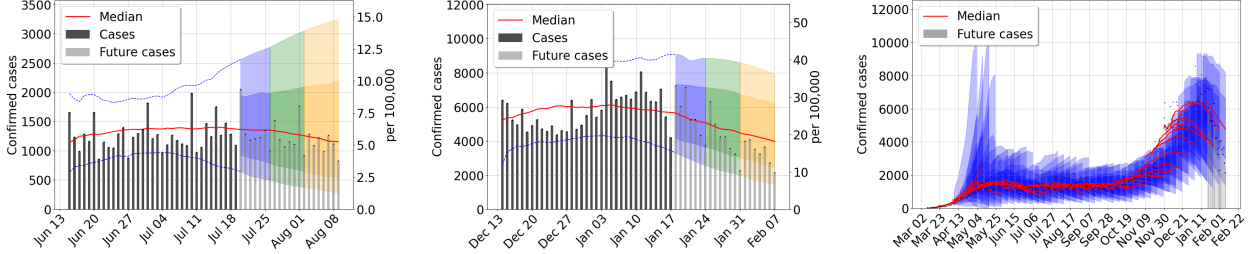


(a) Forecast using data from April 20 to May 24, 2020.

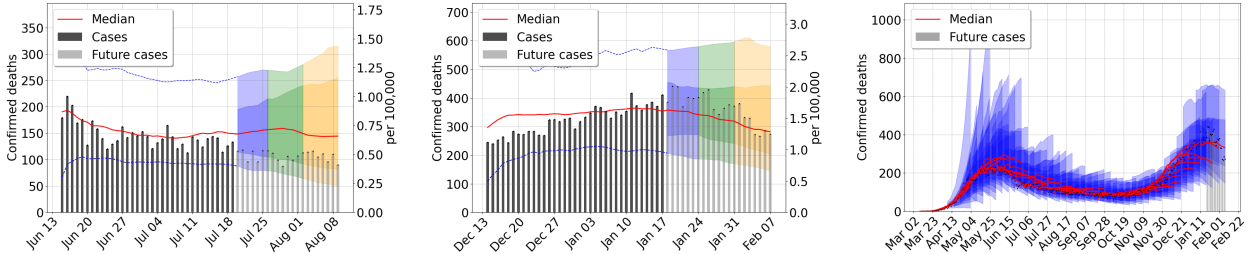


(b) The previous forecastings were superimposed.

Figure 4: Outbreak analysis for Mexico City metropolitan area. From left to right, confirmed cases and deaths. Central red lines indicate the median incidence forecast. The darker shaded region indicates the interquartile forecast range, and the lighter shaded region indicates the 5–95th percentile range. All displayed forecast durations are 21 days from the point of prediction. We stress that nowcasting is very accurate throughout examples presented here and in the SM.



(a) From left to right, forecast for confirmed cases using data from June 15 to July 19, 2020, and data from December 14, 2020, to January 17, 2021. All the previous forecasting was superimposed.



(b) From left to right, forecast for confirmed deaths using data from June 15 to July 19, 2020, and data from December 14, 2020, to January 17, 2021. All the previous forecasting was superimposed.

Figure 5: Outbreak analysis for Mexico City metropolitan area. From left to right, confirmed cases and deaths. Central red lines indicate the median incidence forecast. The darker shaded region indicates the interquartile forecast range, and the lighter shaded region indicates the 5–95th percentile range. All displayed forecast duration are 20 days from the point of prediction.

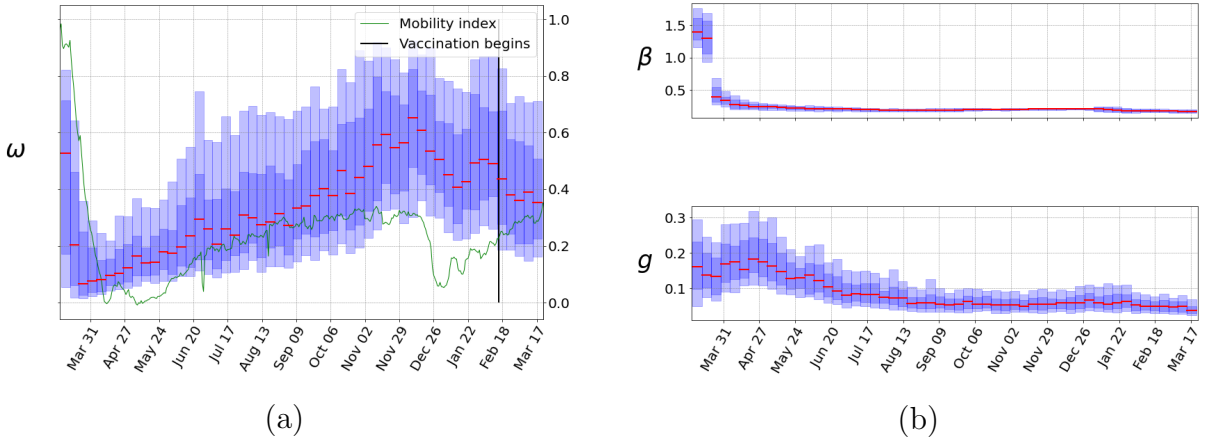


Figure 6: Outbreak analysis for Mexico City metropolitan area. In panel (a), it is apparent that the social media based unique mobility index is an adequate proxy of model predicted effective population proportion ( $\omega$ ). In panel (b) top, contact rate after lockdown ( $\beta$ ) suggests contact rate is independent of  $\omega$ , and (b) bottom shows the fraction of those infected dying at the hospital ( $g$ ). Central red lines indicate median incidence forecast. Darker shaded region indicates forecast interquartile range, and lighter shaded region indicates 5–95th percentile range.

## 4.1 Forecast performance

This paper presents the probabilistic one to four-week ahead forecasts of the total number of confirmed cases and deaths due to COVID-19 from early-mid March 2020 to February 2021 for all Mexican states. In our forecasting algorithm, we take into account reporting delays of 11 days in the past. Therefore, the earliest forecasts are, in fact, nowcasting (“predictions of the past present”). This becomes important to sense the most recent infection trends and could be a deciding factor in managing social distancing policies.

We evaluated our forecast performance using prediction interval coverage for two metrics; the 25% to 75% and the 10% to 90% interquartile. We call them the 50%, or interquartile and 80% forecast cones, respectively. The prediction interval coverage is calculated by counting the frequency with which the prediction interval contains the eventually observed outcome. In a model that accurately characterizes uncertainty, the prediction interval level will correspond closely to the frequency of eventually observed outcomes that fall within that prediction interval. For example, finally, observed values should be within the interquartile prediction interval approximately 50% of the time.

In Figure 7 we present the result of our analysis of the 1-4 week forecast performance in the Mexico City metropolitan area (ZVMX). The left figures show the weakly performance for the 50% and 80% cones, while the figure on the right shows a slope-graph of the weekly performance average of the one to four-week forecasts measured for the 50% and 80% cones metrics. In the latter figure, we included the performance measured for all 32 states as a comparison. The performance measure shows variability among the different states (see also Figures S12 to S15 in SM), but in every case, the performance is above 50 and 40 percent for confirmed cases and deads, respectively. Therefore, we are confident to say that our model characterizes uncertainty accurately in all cases.

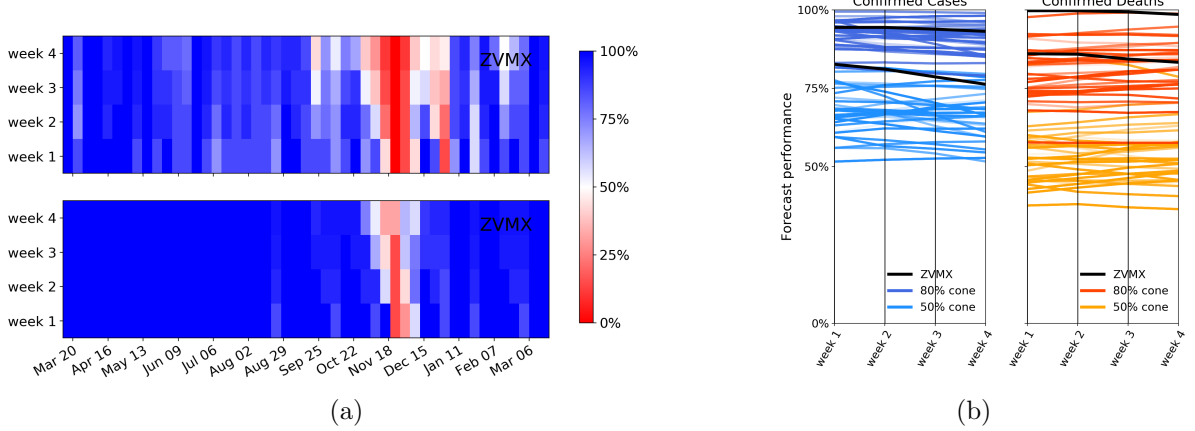


Figure 7: In panel (a), we present a heat-map of the 1-4 week forecast performance in the Mexico City metropolitan area (ZVMX). The top and bottom figures show the performance measure for the 50% and 80% prediction cones, respectively. Predictions performance values are above 80 and 90 percent for all times in both cases outside the second pandemic peak’s exponential growth period -between November and December 2020- where prediction performance decreases. In panel (b), we present a slope-graph of the average weekly forecast performance for all 32 states in Mexico. Each line connects a state’s average performance for 1 to 4 weeks forecast. Darker and lighter colors correspond to the performance measured for the 50% and 80% prediction cones, respectively. We also include ZVMX performance in black color. Left and right plots correspond to confirmed cases and confirmed deaths, respectively. In all cases, the forecast’s performance decreases slightly with the prediction length. The 50% cone has a performance value between 50 and 80 percent, and the 80% cone has a corresponding value between 80% and 100% for confirmed cases. In the case of deaths, the 50% and 80% cones have performance values between 40% and 60% and between 60% and 100%, respectively.

## 5 Discussion and conclusions

The current COVID19 pandemic has posed significant challenges in scientific research. In mathematics, forecasting and modeling an ongoing epidemic outbreak is a major problem. Although some general modeling methods are available, such as Bayesian inference and data assimilation schemes, thought-out modeling decisions are needed for specific cases. Clear-cut methodologies in the modeling processes remain unclear. Identification of general principles and modeling strategies will improve our forecasting capabilities.

In this paper, we propose a general Bayesian sequential data assimilation method. Updates in the dynamical system’s evolution are given as posterior distributions of both model parameters and state variables as new epidemic records become available. New prior models are defined from the current parameters and state variables posterior distributions on a sliding time window. Within each sliding window, posterior distributions are computed beyond the available epidemic records to produce forecasts. We argue that if the underlying epidemic and transmission models are derived from first principles under sensible epidemiological assumptions, we should expect reliable forecasts, provided a stable and consistent stream of data to inform the statistical observation model is available. The case of the COVID-19 pandemic in this manuscript supports our claim.

In many studies [1,2,7], inference schemes assume constant model parameters, failing to recognize

the non-autonomous nature of the prolonged COVID19 pandemic outbreak. Public behavior, such as mask-wearing, change model transmission parameters, while lockdown measures changes the poll of susceptible individuals. Moreover, the case and hospital fatality rates also depends on the health workers' learning curve to treat the disease. Other studies [15, 27] that consider time-dependent parameters lack a well-designed moving-in-time data assimilation scheme.

We argue that our Bayesian filtering method can effectively capture the parameter's time evolution, achieving an information balance between the outbreak's entire history and its latest short-term behavior. Moreover, for the usual SEIRD type dynamical models, long time series epidemiological records pose a hard inference problem. Some authors (e.g. [7]) address this issue using models with more parameters and complex dynamical systems structures that try to capture the changing landscape. We maintain that our model poses a sensible alternative to this approach, where a more unambiguous interpretation of few time-dependent inferred parameters in epidemiological scenarios becomes feasible.

We can derive some insights into the current COVID-19 pandemic from our model. In SEIRD type models, there exists a confounding effect between susceptible individuals' pool and the infections contact rate [7]. Our model disentangles these parameters after the first wave's exponential growth periods. For second waves, part of these parameters are "learned," and our method produces more accurate estimates. The evidence we have gathered for more than 70 cities and the 32 states in Mexico shows a clear difference between the time-dependent behavior of the infection contact rate  $\beta$  and the susceptible pool represented by  $\omega$ . Moreover, the relatively constant value of  $\beta$  in all cases implies that this quantity is mainly disease dependent, while the changes in  $\omega$  are a proxy of peoples' response to mobility restrictions such as lockdown and lockdown-release measures. A piece of further evidence is given by the correlations between  $\omega$  and the mobility index derived from social media tracking. As a proxy of mobility, we notice that  $\omega$  represents the complex network of people's contacts in a metropolitan area with a single number. Hence, its significant uncertainty for almost all times.

The hospital fatality rate  $g$  (the proportion of COVID19 in-patients that eventually die) is also inferred as part of the model. Interestingly, its value declines over time, with a slight and steady further decline starting in February 2021 in some cities. The last reduction is consistent with the local vaccination campaigns on the elderly population. The evidence is still thin and a more definite picture should emerge in the following months. Mask-wearing is widely accepted as a primary measure to prevent contagion. In our model, changes in this behavior should be reflected in the transmission rate  $\beta$ . Unfortunately, up to our knowledge, there are no reliable studies on the mask-wearing practices –or other personal hygiene measures– that we can compare or estimates on  $\beta$  with. Nevertheless, if that is the case, our results show that the population has maintained this practice rather constant through the pandemic.

In a forecasting algorithm like the one presented here, a reliable stream of information is essential. Well-defined epidemiological data records are necessary for reliable inferences. In Mexico, the federal testing policy has been consistent throughout the pandemic. Starting on April 2020, only positive tests at hospital admissions are reported [28], while open population tests are kept in separate records. Therefore, the data used in the model has a constant and consistent bias, as can be observed from the almost constant in time positivity test rate (see Figure S1 in SM). Therefore, application of the present model to other countries and cities would require a careful analysis of the corresponding testing policies that may affect forecast and inferred parameters due to non constant biases.

Well-designed Bayesian data assimilation schemes for nonlinear dynamical systems such as the epidemiological model presented in the current paper produce a reliable and helpful forecasts. Meaningful insights into the recent COVID19 epidemic outbreak also rose from the proposed modeling strategy. Beyond epidemiology, the introduced principles and methods apply to other non-autonomous dynamical models. The present study is a step towards a more comprehensive

understanding of mathematical forecasting methods; further research is still needed.

## Data reporting

The databases necessary for the estimation of parameters and the codes implemented for the study are available in the github repository

<https://github.com/mdazatorres/Bayesian-sequential-data-assimilation-method>. Analyses were carried out using Python version 3.

## Data sources

Daily COVID-19 confirmed cases and deaths for all Mexican states and Mexico City's metropolitan area. All data are publicly available at <https://datos.covid-19.conacyt.mx>, and therefore did not require ethical approval of an institutional review board nor written informed consent. All analyses were conducted with data updated to May 2, 2020.

## Acknowledgments

The authors are partially founded by CONACYT CB-2016-01-284451 grant. AC was partially supported by UNAM PAPPIT-IN106118 grant. MLDT was funded by FONDECYT 296737 “CONSORCIO EN INTELIGENCIA ARTIFICIAL”.

## References

- [1] Jason Asher. Forecasting ebola with a regression transmission model. *Epidemics*, 22:50–55, 2018.
- [2] Andrea L Bertozzi, Elissa Franco, George Mohler, Martin B Short, and Daniel Sledge. The challenges of modeling and forecasting the spread of covid-19. *arXiv preprint arXiv:2004.04741*, 2020.
- [3] Mario Castro, Saúl Ares, José A Cuesta, and Susanna Manrubia. The turning point and end of an expanding epidemic cannot be precisely forecast. *Proceedings of the National Academy of Sciences*, 117(42):26190–26196, 2020.
- [4] Claus O Wilke and Carl T Bergstrom. Predicting an epidemic trajectory is difficult. *Proceedings of the National Academy of Sciences*, 2020.
- [5] Steven G Krantz and Arni SR Srinivasa Rao. Level of underreporting including underdiagnosis before the first peak of covid-19 in various countries: Preliminary retrospective results based on wavelets and deterministic modeling. *Infection Control & Hospital Epidemiology*, 41(7):857–859, 2020.
- [6] Hien Lau, Tanja Khosrawipour, Piotr Kocbach, Hirohito Ichii, Jacek Bania, and Veria Khosrawipour. Evaluating the massive underreporting and undertesting of covid-19 cases in multiple global epicenters. *Pulmonology*, 27(2):110–115, 2021.
- [7] Marcos A. Capistran, Antonio Capella, and J. Andrés Christen. Forecasting hospital demand in metropolitan areas during the current covid-19 pandemic and estimates of lockdown-induced 2nd waves. *PLOS ONE*, 16(1):1–16, 2021.
- [8] Logan C Brooks, Evan L Ray, Jacob Bien, Johannes Bracher, Aaron Rumack, Ryan J Tibshirani, and Nicholas G Reich. Comparing ensemble approaches for short-term probabilistic covid-19 forecasts in the us. *International Institute of Forecasters*, 2020.
- [9] Ralf Engbert, Maximilian M Rabe, Reinhold Kliegl, and Sebastian Reich. Sequential data assimilation of the stochastic seir epidemic model for regional covid-19 dynamics. *Bulletin of mathematical biology*, 83(1):1–16, 2021.
- [10] Herbert W Hethcote. The mathematics of infectious diseases. *SIAM review*, 42(4):599–653, 2000.
- [11] Pauline Van den Driessche and James Watmough. Reproduction numbers and sub-threshold endemic equilibria for compartmental models of disease transmission. *Mathematical biosciences*, 180(1-2):29–48, 2002.
- [12] David Champredon, Jonathan Dushoff, and David JD Earn. Equivalence of the erlang-distributed seir epidemic model and the renewal equation. *SIAM Journal on Applied Mathematics*, 78(6):3258–3278, 2018.
- [13] Leonhard Held, Niel Hens, Philip D O’Neill, and Jacco Wallinga. *Handbook of infectious disease data analysis*. CRC Press, 2019.
- [14] Angel N Desai, Moritz UG Kraemer, Sangeeta Bhatia, Anne Cori, Pierre Nouvellet, Mark Herring, Emily L Cohn, Malwina Carrion, John S Brownstein, Lawrence C Madoff, et al. Real-time epidemic forecasting: challenges and opportunities. *Health security*, 17(4):268–275, 2019.

- [15] Graham C Gibson, Nicholas G Reich, and Daniel Sheldon. Real-time mechanistic bayesian forecasts of covid-19 mortality. *medRxiv*, 2020.
- [16] Sarah F McGough, John S Brownstein, Jared B Hawkins, and Mauricio Santillana. Forecasting zika incidence in the 2016 latin america outbreak combining traditional disease surveillance with search, social media, and news report data. *PLoS neglected tropical diseases*, 11(1):e0005295, 2017.
- [17] Cécile Viboud, Kaiyuan Sun, Robert Gaffey, Marco Ajelli, Laura Fumanelli, Stefano Merler, Qian Zhang, Gerardo Chowell, Lone Simonsen, Alessandro Vespignani, et al. The rapidd ebola forecasting challenge: Synthesis and lessons learnt. *Epidemics*, 22:13–21, 2018.
- [18] Yien Ling Hii, Huaiping Zhu, Nawi Ng, Lee Ching Ng, and Joacim Rocklöv. Forecast of dengue incidence using temperature and rainfall. *PLoS Negl Trop Dis*, 6(11):e1908, 2012.
- [19] D. V. Lindley. *Bayesian statistics, a review*. SIAM, Philadelphia, PA, USA, 1972.
- [20] SA Lauer, KH Grantz, Q Bi, FK Jones, Q Zheng, HR Meredith, AS Azman, and NG Reich. 181 lessler j. the incubation period of coronavirus disease 2019 (covid-19) from publicly 182 reported confirmed cases: estimation and application. *Ann Intern Med*, 2020.
- [21] Xuan Jiang, Simon Rayner, and Min-Hua Luo. Does sars-cov-2 has a longer incubation period than sars and mers? *Journal of medical virology*, 92(5):476–478, 2020.
- [22] Quan-Xin Long, Xiao-Jun Tang, Qiu-Lin Shi, Qin Li, Hai-Jun Deng, Jun Yuan, Jie-Li Hu, Wei Xu, Yong Zhang, Fa-Jin Lv, et al. Clinical and immunological assessment of asymptomatic sars-cov-2 infections. *Nature medicine*, 26(8):1200–1204, 2020.
- [23] Robert Verity, Lucy C Okell, Ilaria Dorigatti, Peter Winskill, Charles Whittaker, Natsuko Imai, Gina Cuomo-Dannenburg, Hayley Thompson, Patrick GT Walker, Han Fu, et al. Estimates of the severity of coronavirus disease 2019: a model-based analysis. *The Lancet infectious diseases*, 2020.
- [24] Qifang Bi, Yongsheng Wu, Shujiang Mei, Chenfei Ye, Xuan Zou, Zhen Zhang, Xiaojian Liu, Lan Wei, Shaun A Truelove, Tong Zhang, et al. Epidemiology and transmission of covid-19 in shenzhen china: Analysis of 391 cases and 1,286 of their close contacts. *MedRxiv*, 2020.
- [25] Seth Flaxman, Swapnil Mishra, Axel Gandy, H Juliette T Unwin, Thomas A Mellan, Helen Coupland, Charles Whittaker, Harrison Zhu, Tresnia Berah, Jeffrey W Eaton, et al. Estimating the effects of non-pharmaceutical interventions on covid-19 in europe. *Nature*, 584(7820):257–261, 2020.
- [26] J. A. Christen and C. Fox. A general purpose sampling algorithm for continuous distributions (the t-walk). *Bayesian Analysis*, 5(2):263–282, 2010. cited By 60.
- [27] Evan L Ray, Nutcha Wattanachit, Jarad Niemi, Abdul Hannan Kanji, Katie House, Estee Y Cramer, Johannes Bracher, Andrew Zheng, Teresa K Yamana, Xinyue Xiong, et al. Ensemble forecasts of coronavirus disease 2019 (covid-19) in the us. *MedRxiv*, 2020.
- [28] Dirección General de Epidemiología. *Lineamiento estandarizado para la vigilancia epidemiológica y por laboratorio de la enfermedad respiratoria viral. Abril de 2020*. Secretaría de Salud, 2020.

## Supplementary material

### Testing policy, testing bias, and positivity rate

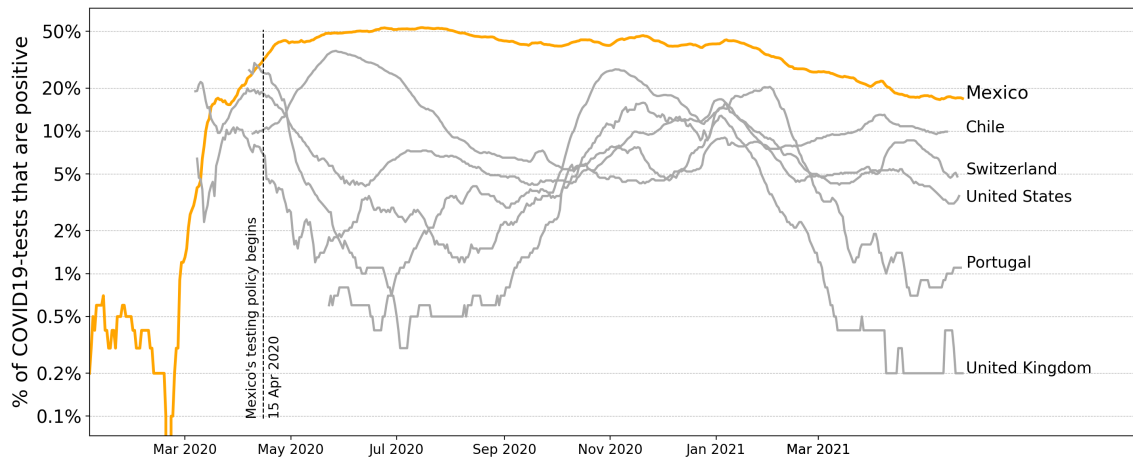


Figure S1: **Percentage of COVID19-tests that are positive for selected countries.** Testing policies during the pandemic have been different among countries and correspond to distinct strategies and objectives. While testing in the open population for contact tracing has been standard in many countries, Mexico's federal health authorities COVID-19 test-policy targets all public hospital admissions exclusively. Starting April 2020, Mexico's testing policy [28] (p. 19, in Spanish) is to test 100% and randomly select 10% of severe and mild suspected cases, respectively. Severe cases correspond to hospital admitted patients and mild cases to ambulatory infections. This restricted testing policy produces a biased sample of positive COVID-19 cases. The upside is that this bias is consistent and constant in time, as the figure confirms. Since infection rates can be estimated better from constant bias samples than from more extensive ones of unknown bias, we have - with this testing policy - a more reliable proxy of the pandemic evolution, better suited for modeling and forecasting. Reasonable estimates of the true number of infected individuals at a given time are impossible to obtain until a characterization of the asymptomatic infection is available. The latter is true for any testing policy besides the rather unrealistic case where the whole population is continuously tested.

## State codes and population considered in epidemic models

State name	Code	Pop.	State name	Code	Pop.
Aguascalientes	AS	1,434,635	Nayarit	NT	1,288,571
Baja California	BC	3,634,868	Nuevo León	NL	5,610,153
Baja California Sur	BS	804,708	Oaxaca	OC	4,143,593
Campeche	CC	1,000,617	Puebla	PL	6,604,451
Chiapas	CS	5,730,367	Querétaro	QO	2,279,637
Chihuahua	CH	3,801,487	Quintana Roo	QR	1,723,259
Coahuila	CL	3,218,720	San Luis Potosí	SP	2,866,142
Colima	CM	785,153	Sinaloa	SL	3,156,674
Durango	DG	1,868,996	Sonora	SR	3,074,745
Guanajuato	GT	6,228,175	Tabasco	TC	2,572,287
Guerrero	GR	3,657,048	Tamaulipas	TS	3,650,602
Hidalgo	HG	3,086,414	Tlaxcala	TL	1,380,011
Jalisco	JC	8,409,693	Veracruz	VZ	8,539,862
Estado de México(*)	MC	4,640,934	Yucatán	YN	2,259,098
Michoacán	MN	4,825,401	Zacatecas	ZS	1,666,426
Morelos	MS	2,044,058	Mexico city area(*)	ZVMX	21,942,666

Table S1: State names, their corresponding codes and population sizes used in our examples, see [https://en.wikipedia.org/wiki/Administrative\\_divisions\\_of\\_Mexico](https://en.wikipedia.org/wiki/Administrative_divisions_of_Mexico) for maps and further details. (\*) Mexico's City metropolitan area, with about 22 million inhabitants, includes some counties that do not belong to the official Mexico's City federal division which only has 8 million inhabitants. As this does not make sense for epidemic modeling, in this study, we define ZVMX as Mexico's City metropolitan area and include the corresponding population of the nearby states. Notably, for the “Estado de Mexico” (MC), we include 12 million inhabitants who live in the ZVMX and remove them from MC.

## Estimates for model parameters for all Mexican states and Mexico City's metropolitan area

## Posterior distributions for the time dependent susceptible pool $\omega$

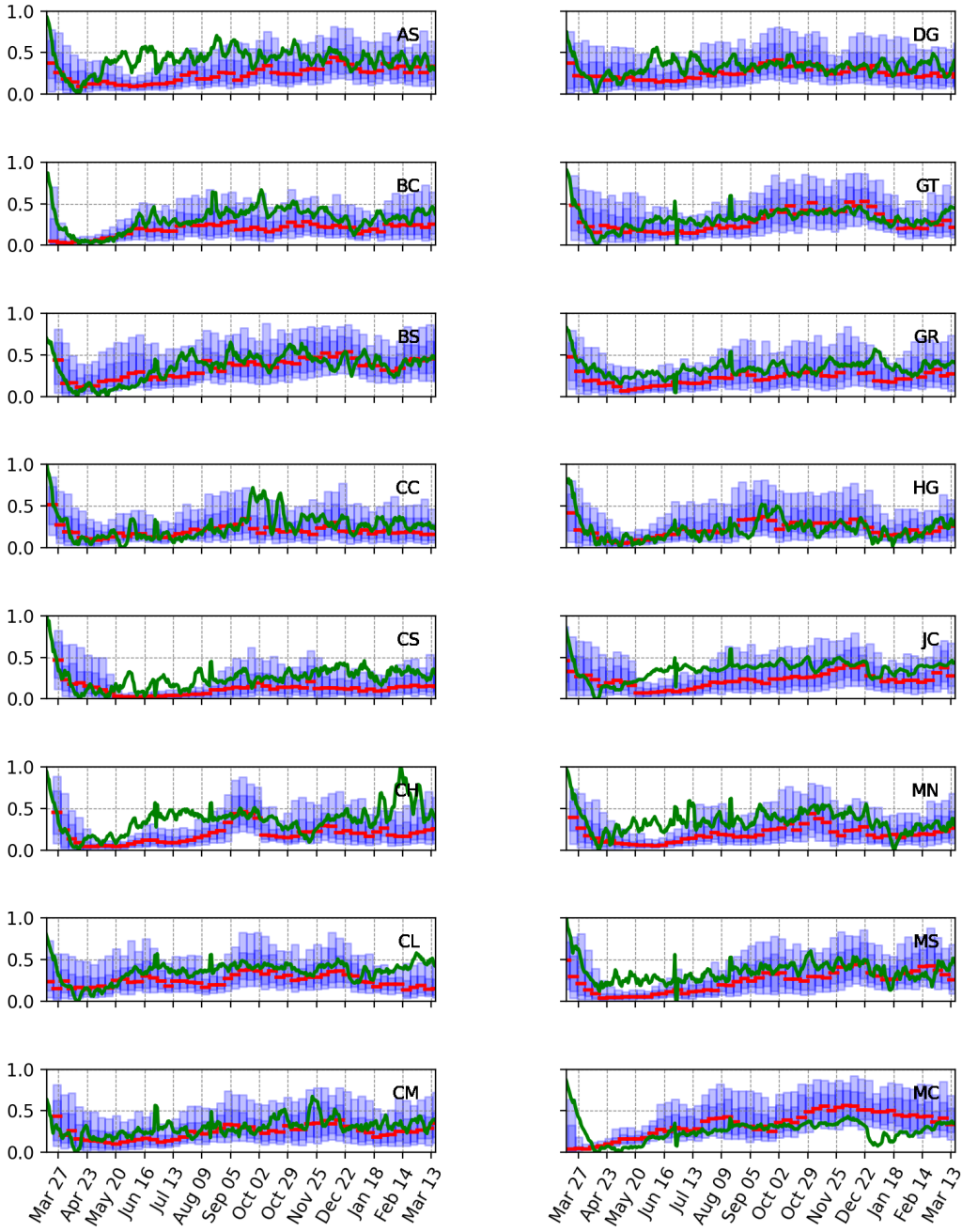


**Figure S2: Posterior distributions for the time dependent susceptible pool  $\omega$ .** We present the weekly posterior distributions for the first 16 Mexican states, with colored vertical box-plots. Light blue is the 10% to 90% quantile range and dark blue are the interquartile ranges; the red lines are the medians. We also added a mobility index (green line, arbitrary units) derived from social media tracking. The susceptible pool of people participating in the epidemic in our model  $\omega$ , indeed only estimated using the epidemic data, seems to correlate (sometimes remarkably well) the mobility index in the corresponding areas. See also Figure S3.

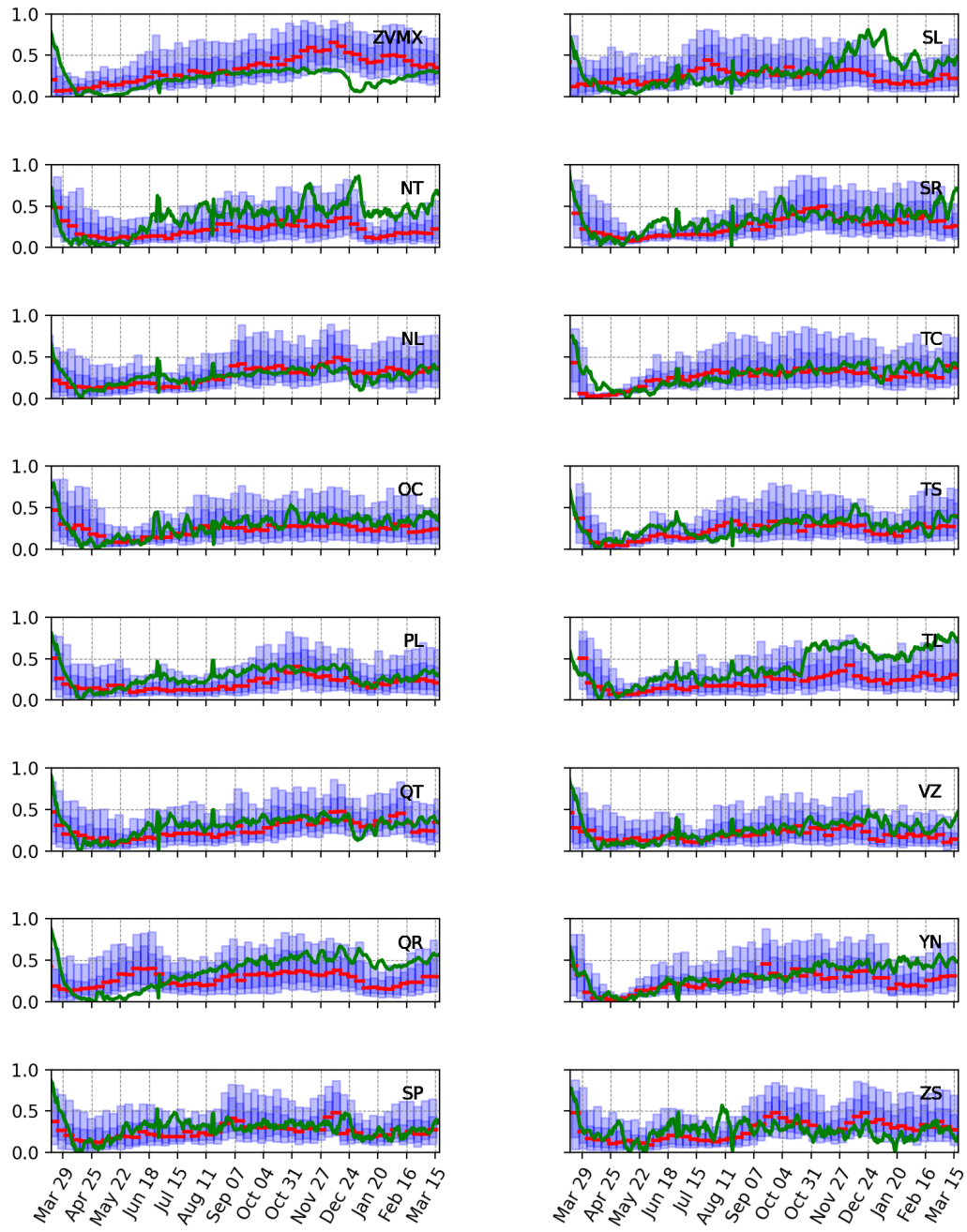


**Figure S3: Posterior distributions for the time dependent susceptible pool  $\omega$ .** We present the weekly posterior distributions for Mexico city metro area and the remaining 15 Mexican states, see Figure S2 for details.

## Posterior distributions for the Infection Contact rate $\beta$

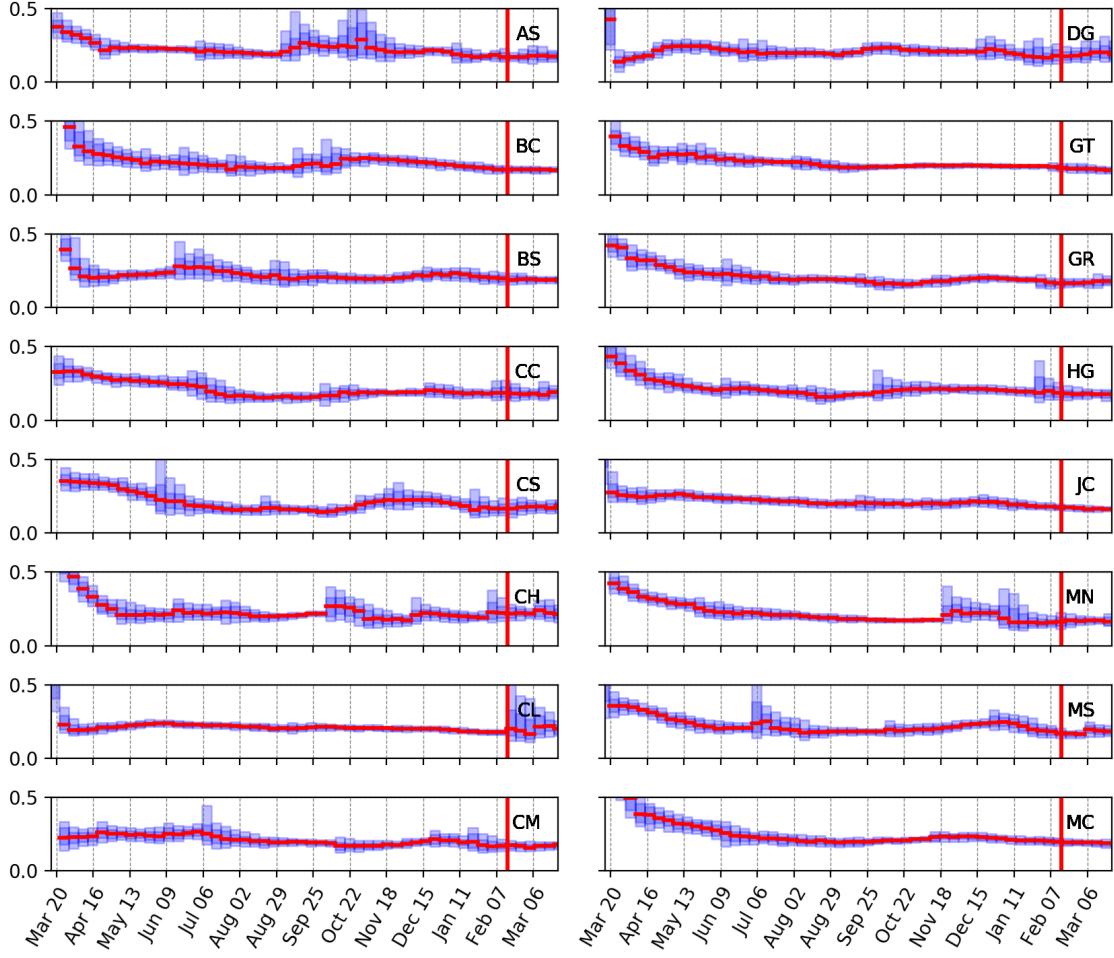


**Figure S4: Posterior distributions for the Infection Contact rate  $\beta$ .** We present the weekly posterior distributions for the first 16 Mexican states for  $\beta$ , displayed as vertical box plots (see Figure S2 for details). The vertical red line marks the day vaccination began. Despite the variability in population, epidemic outbreak history, and other socioeconomic factors, the estimate of Infection Contact rate  $\beta$  show a relatively equal value in all cases. This evidence, combined with the observed variability in the pool of susceptible individuals  $\omega$ , would imply that this quantity is mainly disease dependent. The uncertainty of these posteriors increases in the wave's exponential growth periods, where a confounding effect between  $\omega$  and  $\beta$  exists [7]. See also Figure S5.

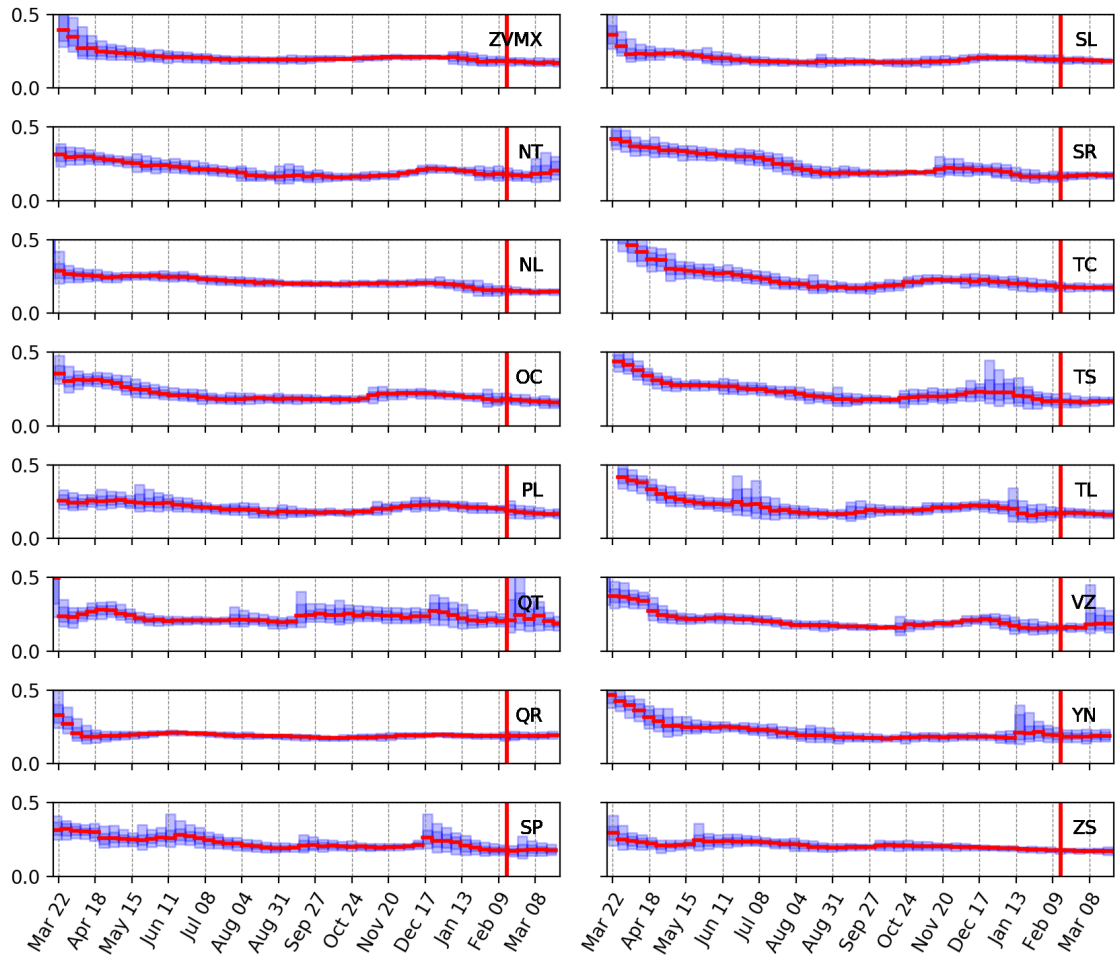
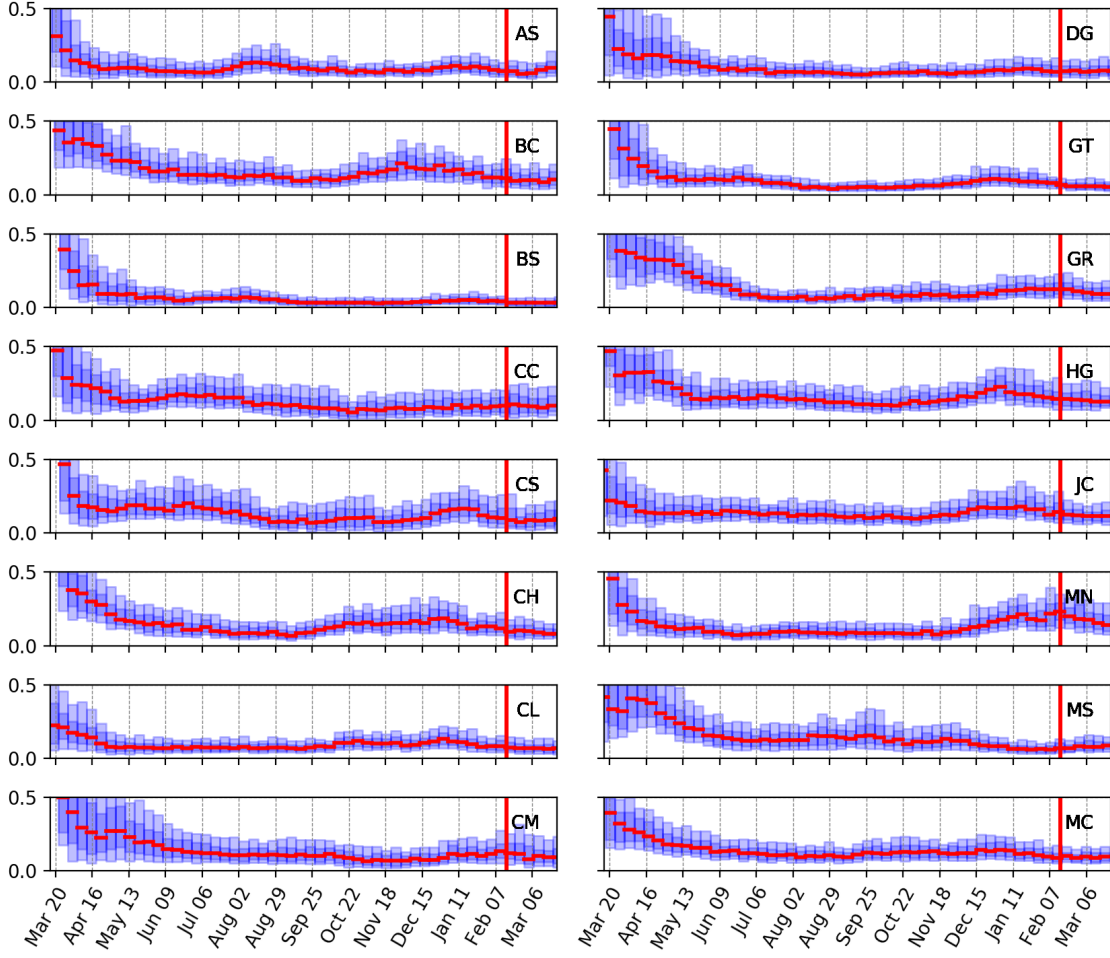


Figure S5: **Posterior distributions for the Infection Contact rate  $\beta$ .** Weekly posterior distributions for  $\beta$ , for Mexico city metro area and the remaining 15 Mexican states, see Figure S4 for details.

## Posterior distributions for the Hospital Fatality rate $g$



**Figure S6: Posterior distributions for the Hospital Fatality rate  $g$ .** We present the weekly posterior distributions for the first 16 Mexican states for  $g$ , displayed as vertical box plots (see Figure S2 for details). Interestingly, its value declines over time, with a slight and steady further decline starting in February 2021 in some cities. It could be argued that last reduction is consistent with the local vaccination campaigns on the elderly population. See also Figure S7.

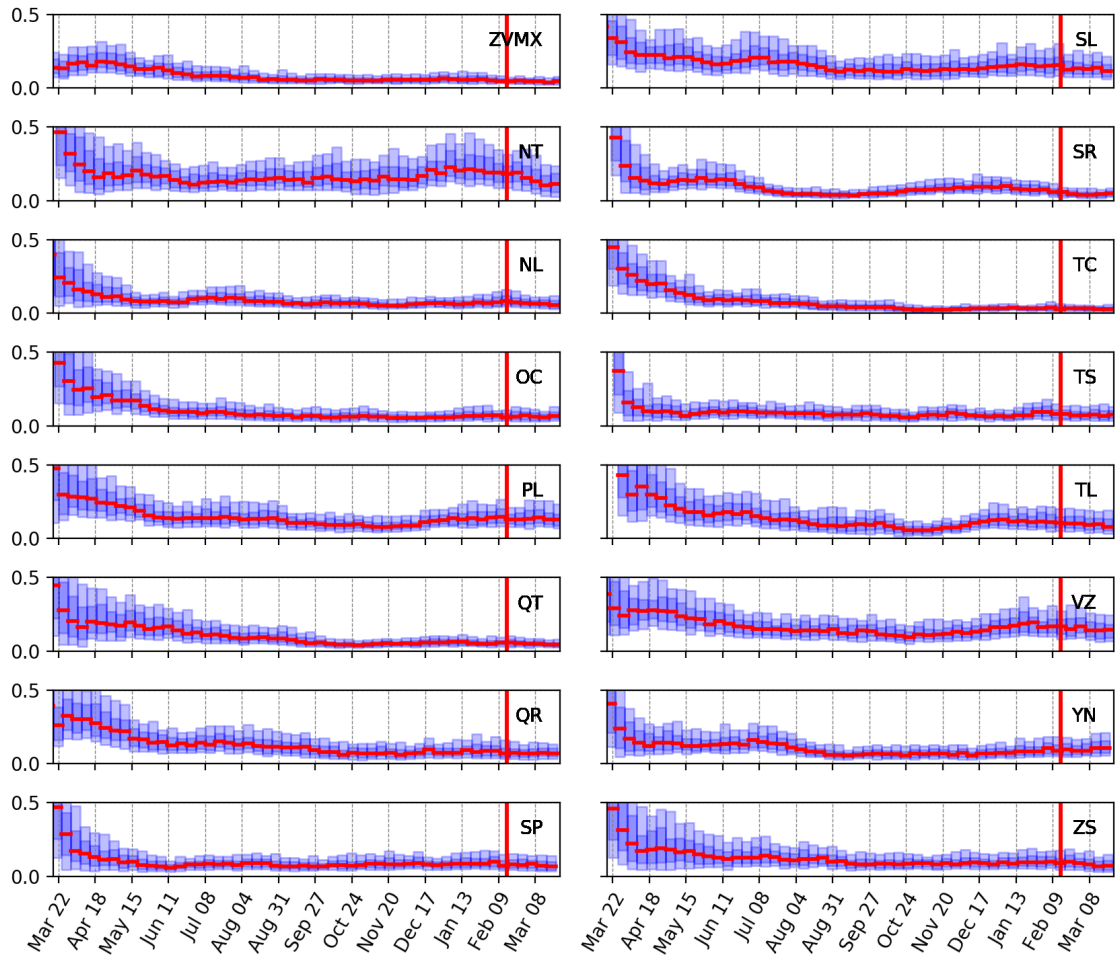


Figure S7: **Posterior distributions for the Hospital Fatality rate  $g$ .** Weekly posterior distributions for  $g$ , for Mexico city metro area and the remaining 15 Mexican states, see Figure S6 for details.

## Forecast results for all Mexican states and Mexico City's metropolitan area

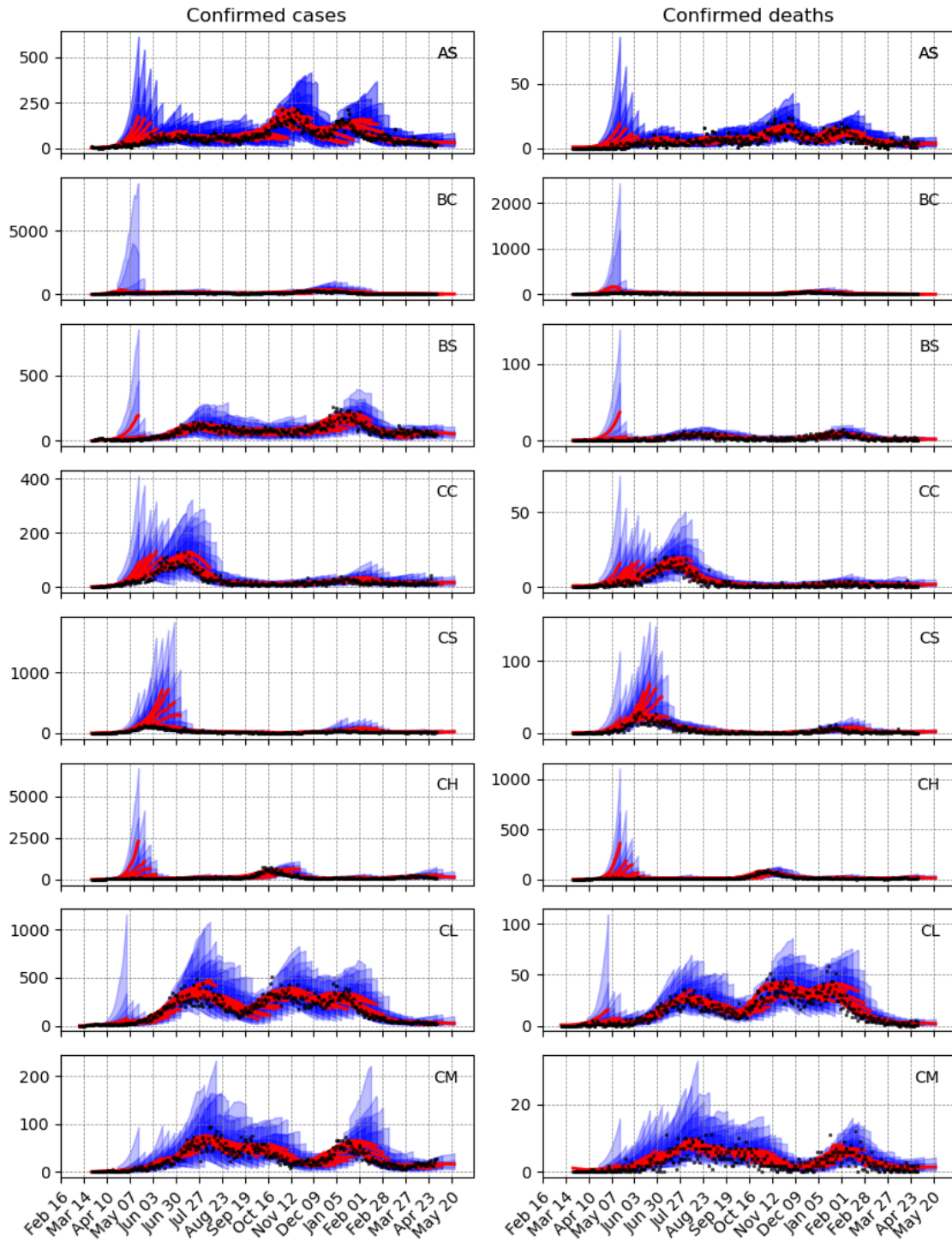


Figure S8: **Forecast results** for all Mexican states and Mexico City's metropolitan area. Left column, confirmed cases, and right column confirmed deaths. The three week posterior predictive distribution is depicted, for each of the weekly moving forecasts windows. Central red lines indicate the median incidence forecast. The darker shaded region indicates the interquartile forecast range, and the lighter shaded region indicates the 10% to 90% quantile range. See also Figures S9, S10 and S11.

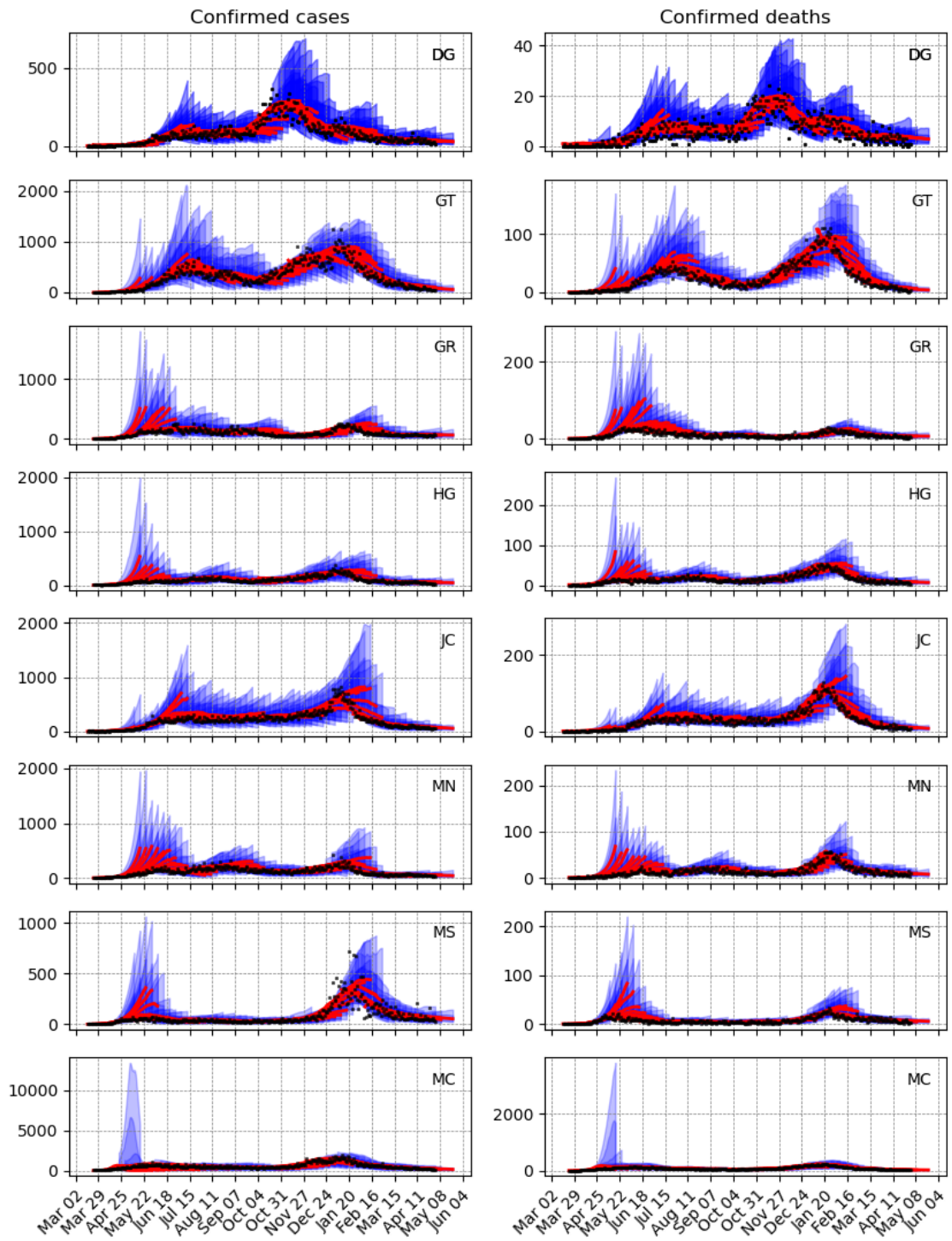


Figure S9: **Forecast results** for all Mexican states, see Figure S8 for details.

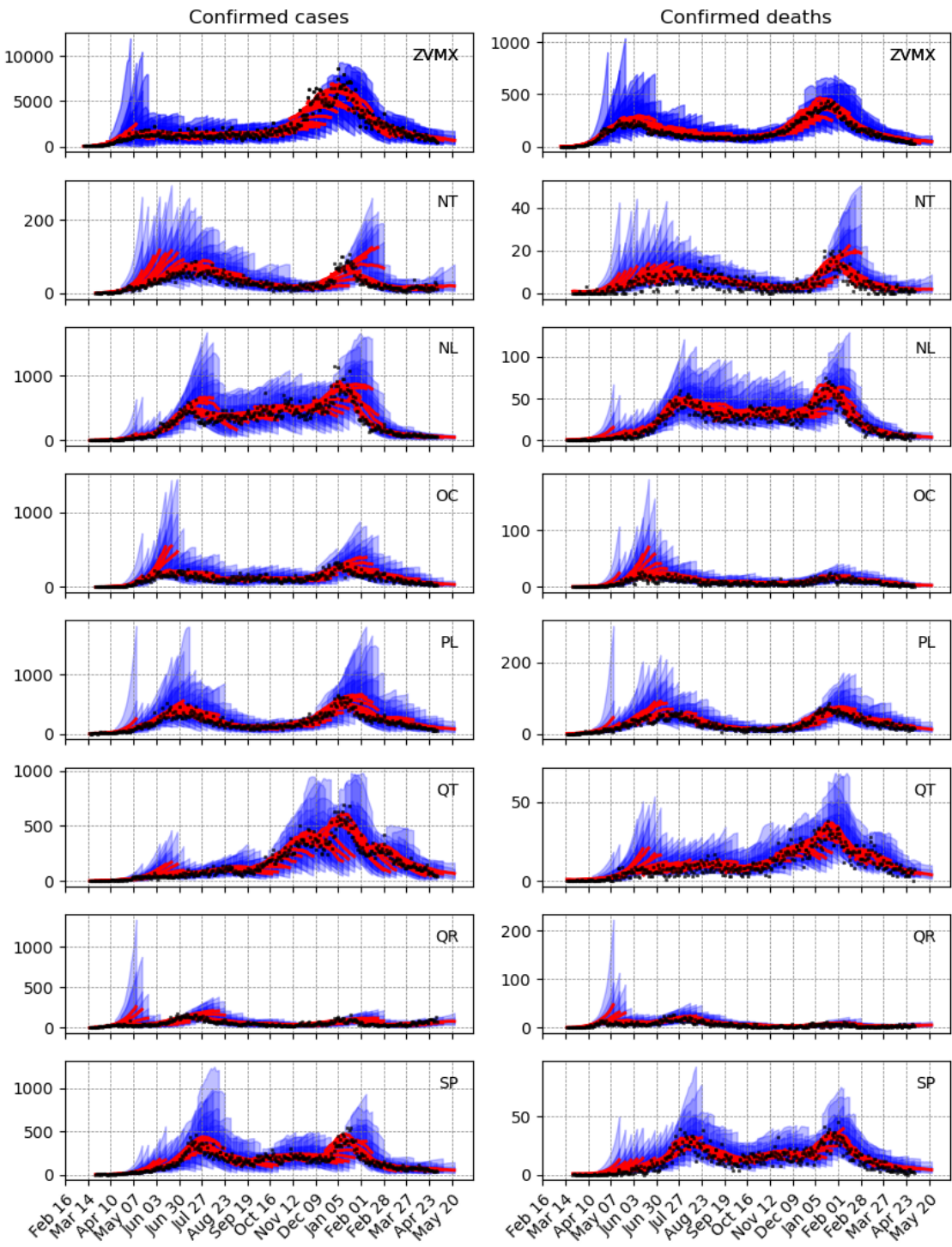


Figure S10: **Forecast results** for all Mexican states, see Figure S8 for details.

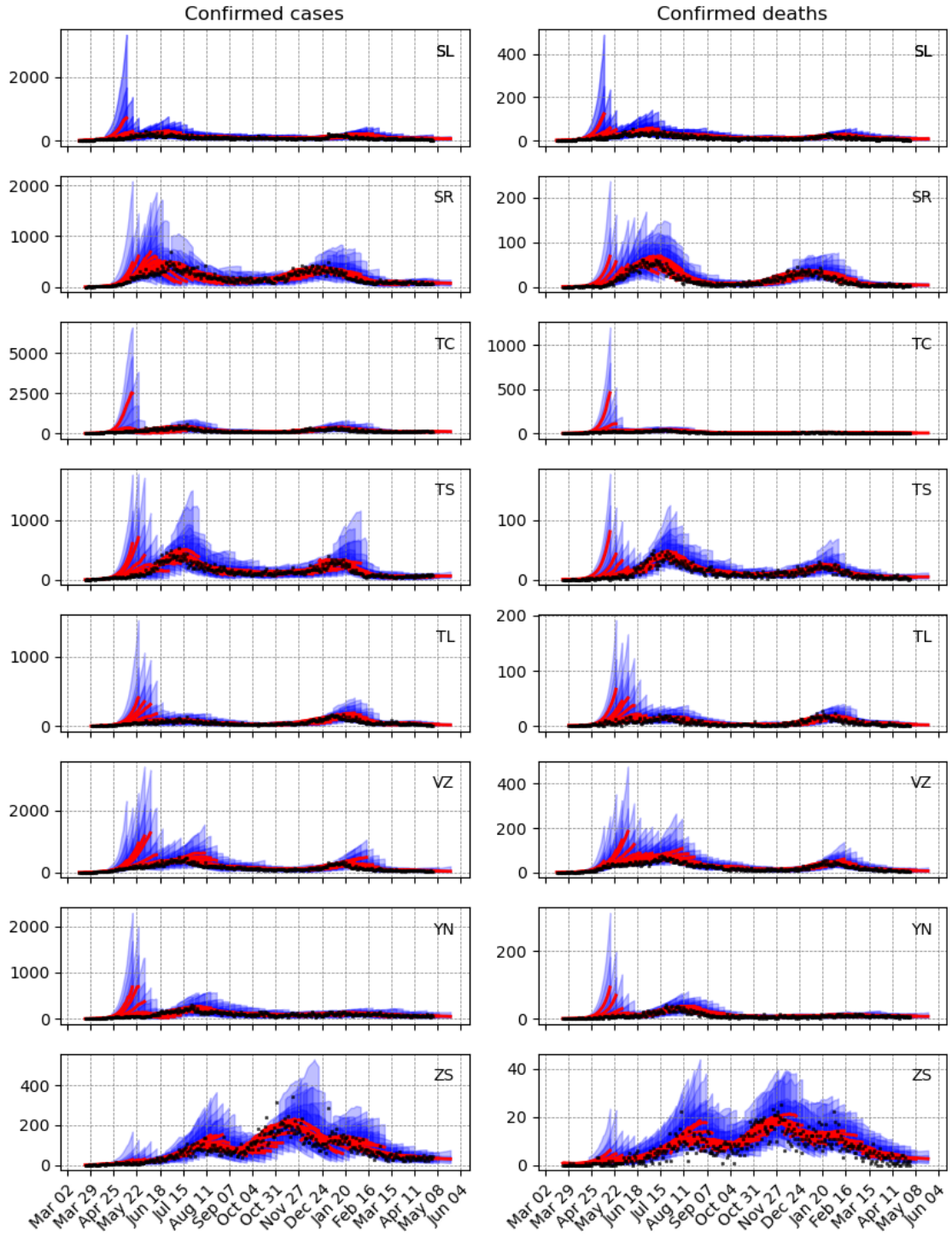
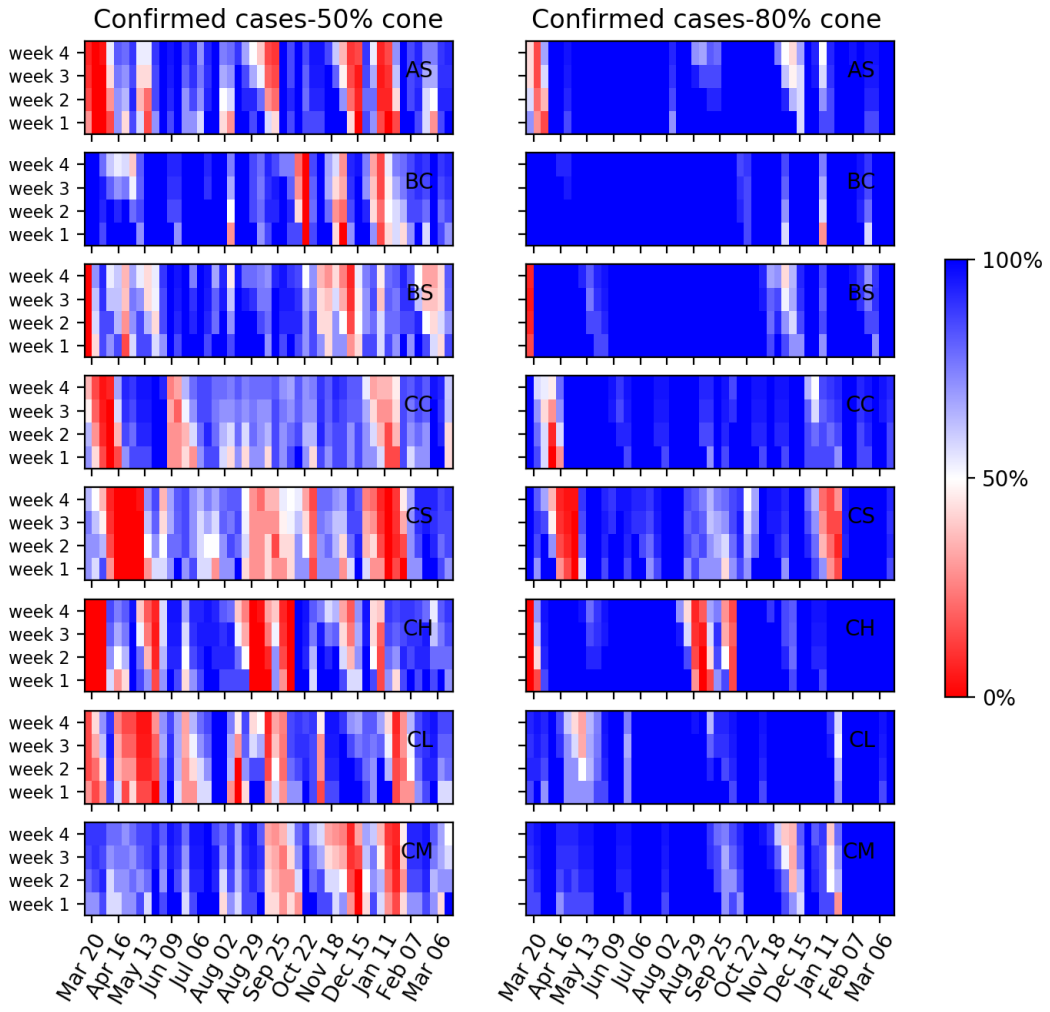


Figure S11: **Forecast results** for all Mexican states, see Figure S8 for details.

## Forecast performance for all Mexican states and Mexico City's metropolitan area



**Figure S12: Heatmap of the one to four week forecasts' performance of confirmed cases for all Mexican states and Mexico City's metropolitan area.** Left and right columns show the performance measure for the 50% (posterior interquartile range) and 80% (10% to 90% quantile range) prediction cones, respectively. Vertically colors are almost constant, showing low sensitivity concerning the prediction length. Prediction performance varies by state and in time, but we have good forecasting performance outside the exponential growth stages in the different pandemic waves, in most cases. See also Figures S13, S14 and S15 and also analogous forecasts' performance panels for confirmed deaths in Figures S16, S17, S18 and S19.

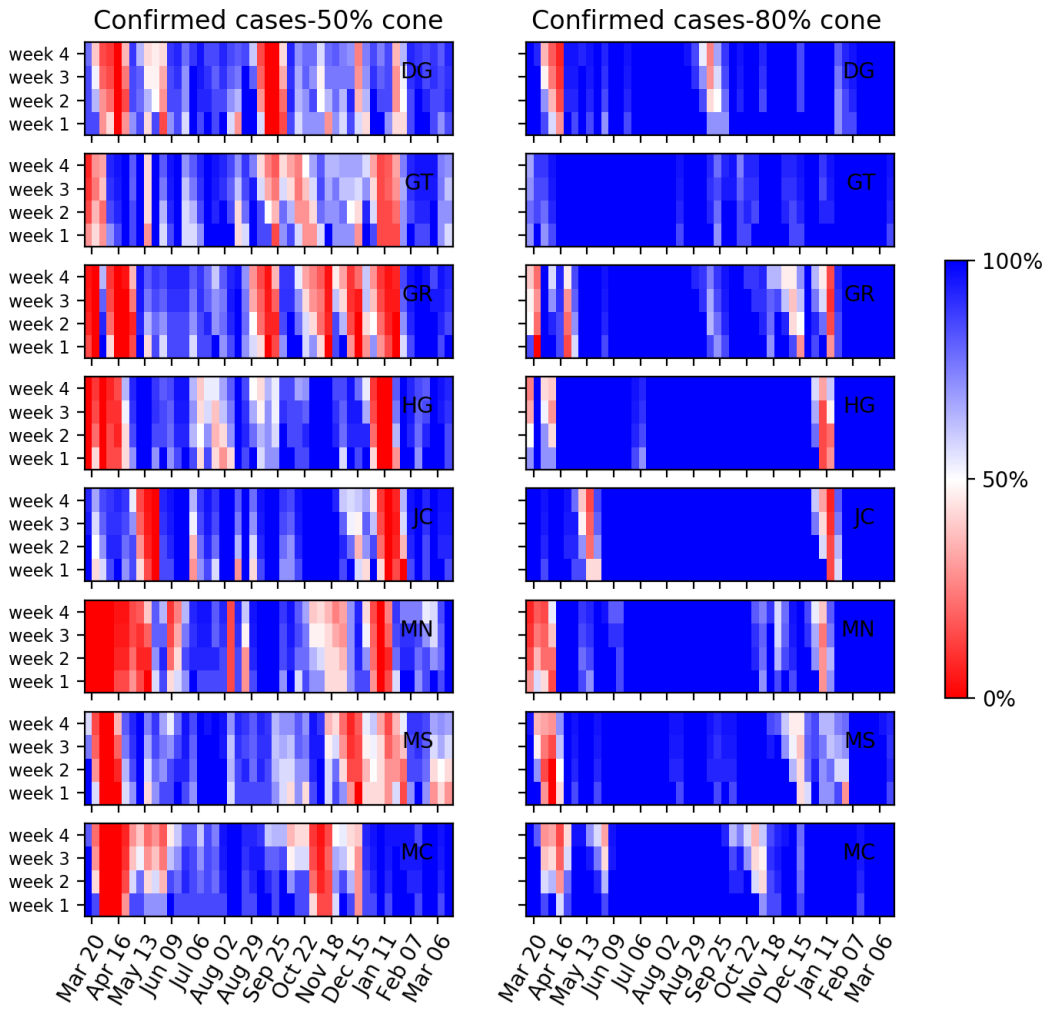
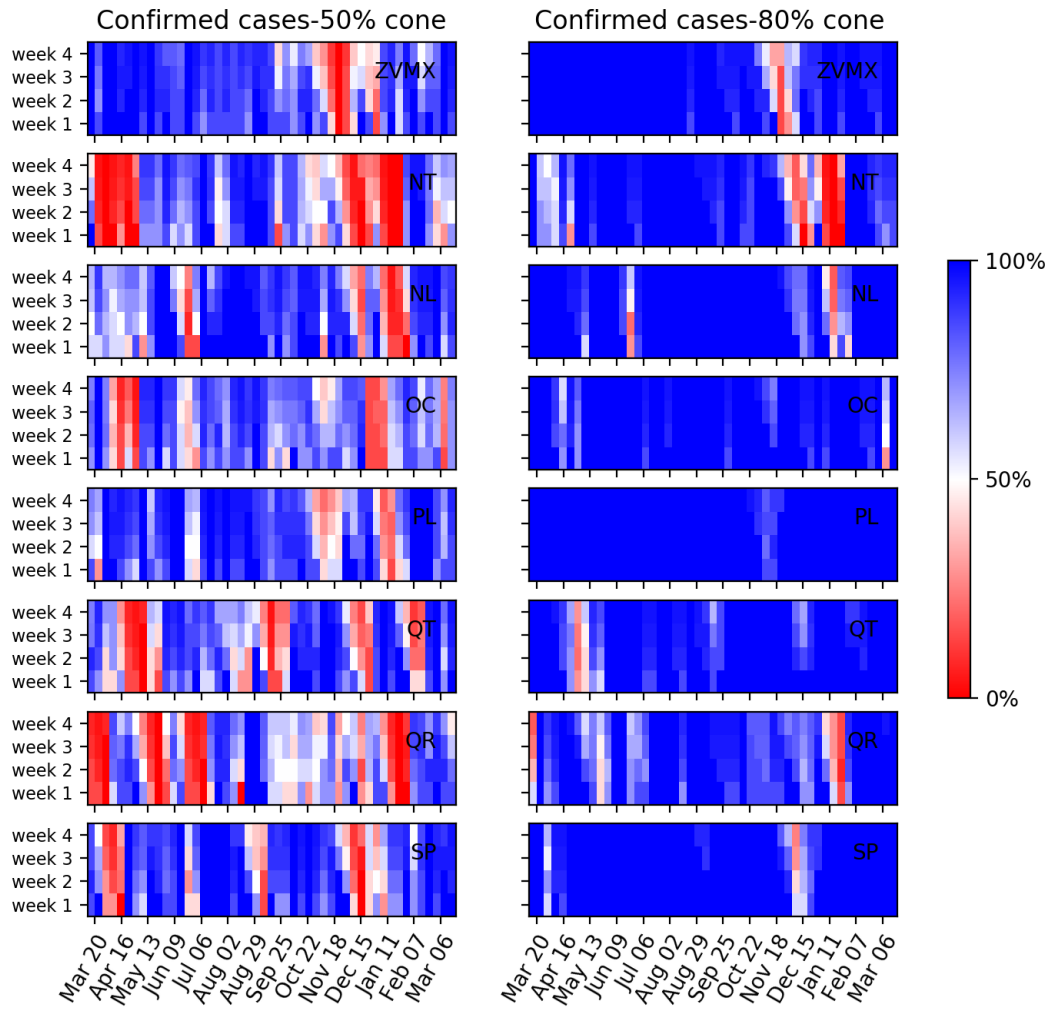


Figure S13: **Heatmap of the one to four week forecasts' performance of confirmed cases**, see Figure S12 for details.



**Figure S14: Heatmap of the one to four week forecasts' performance of confirmed cases, see Figure S12 for details.**

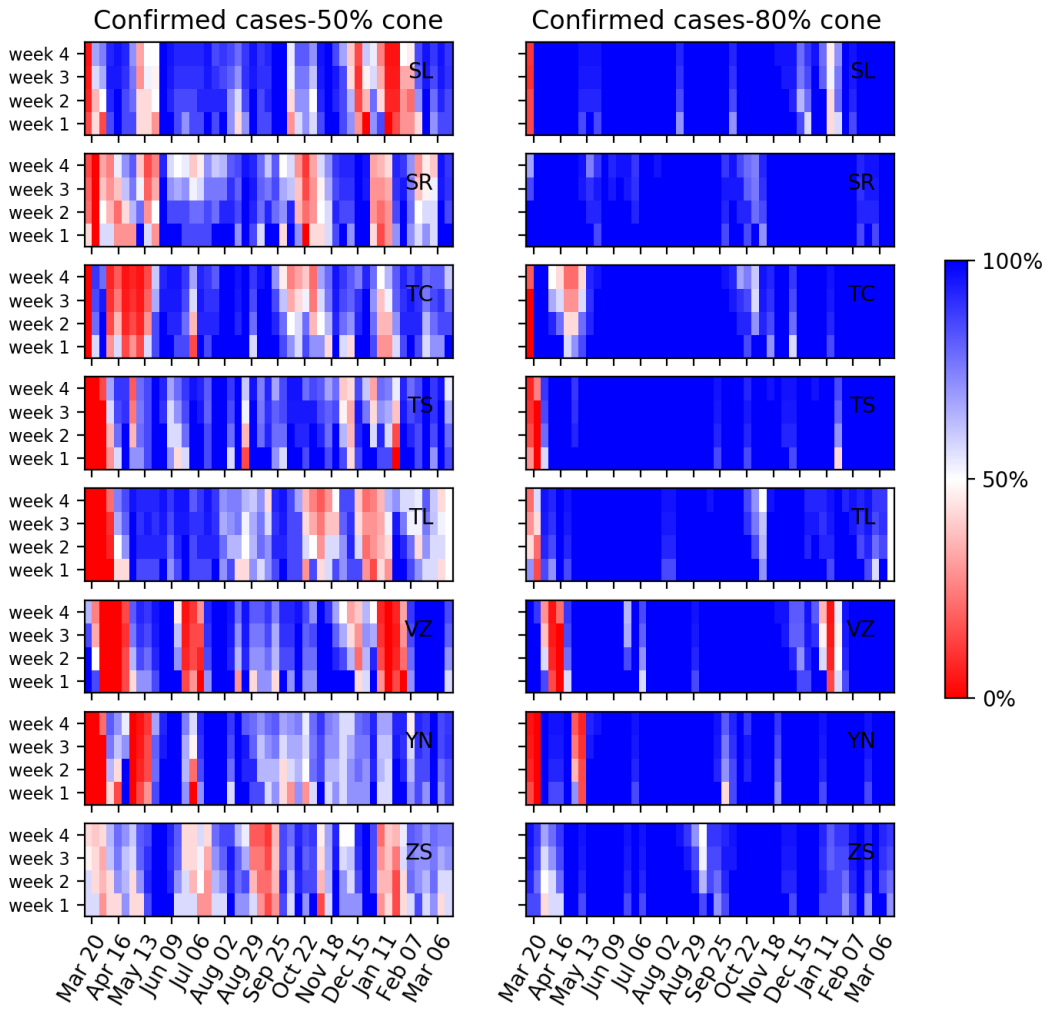
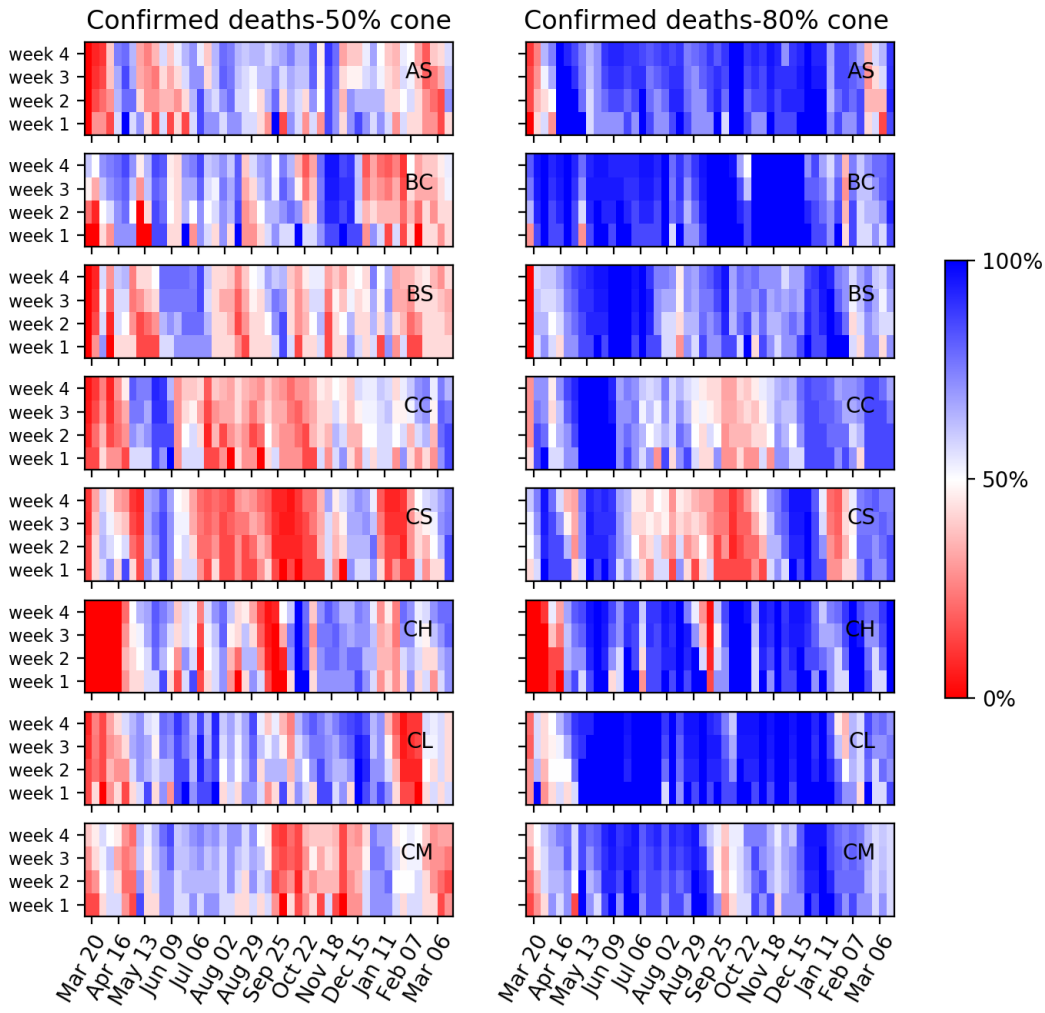


Figure S15: **Heatmap of the one to four week forecasts' performance of confirmed cases**, see Figure S12 for details.



**Figure S16: Heatmap of the one to four week forecasts' performance of confirmed deaths for all Mexican states and Mexico City's metropolitan area.** Left and right columns show the performance measure for the 50% (posterior interquartile range) and 80% (10% to 90% quantile range) prediction cones, respectively. Vertically colors are almost constant, showing low sensitivity concerning the prediction length. Prediction performance varies by state and in time, but we have good forecasting performance outside the exponential growth stages in the different pandemic waves, in most cases. See also Figures S17, S18 and S19.

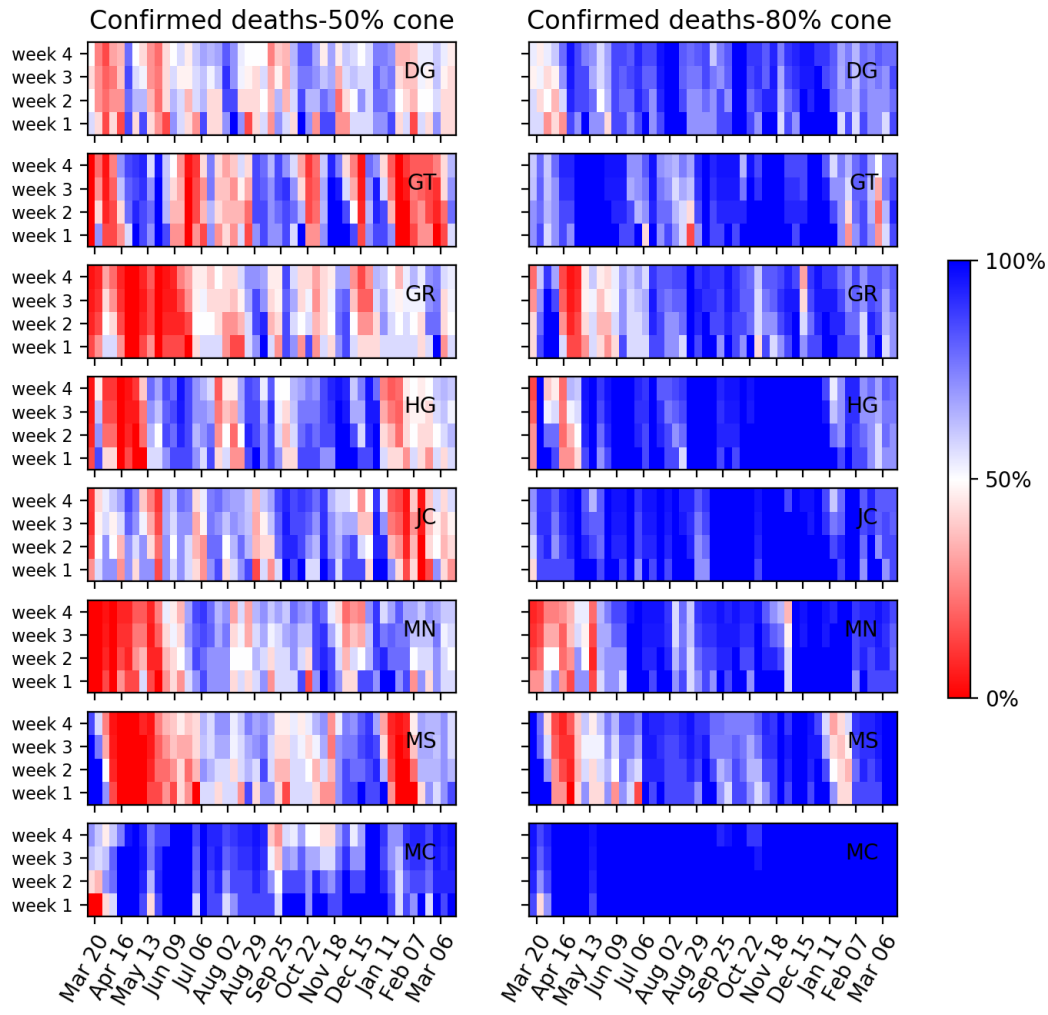


Figure S17: **Heatmap of the one to four week forecasts' performance of confirmed deaths**, see Figure S16 for details.

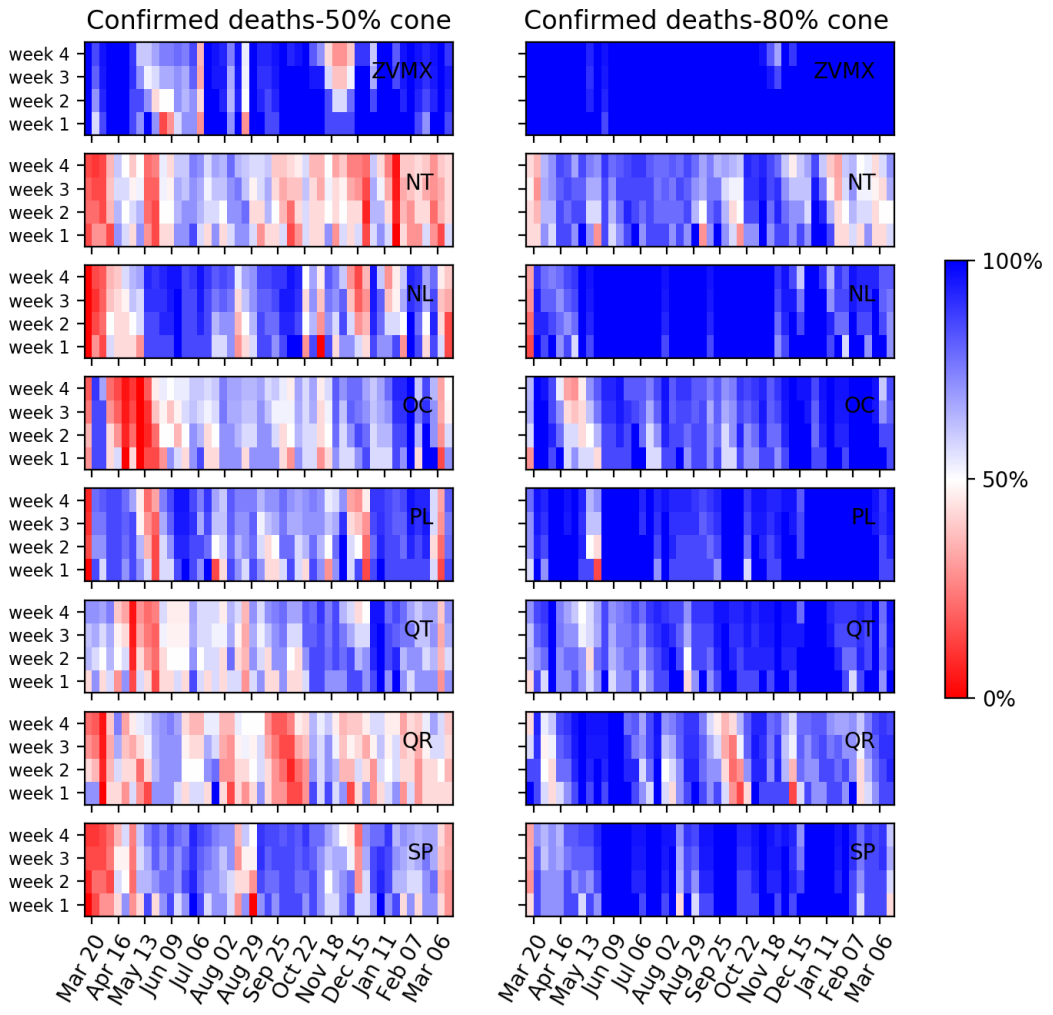


Figure S18: **Heatmap of the one to four week forecasts' performance of confirmed deaths**, see Figure S16 for details.

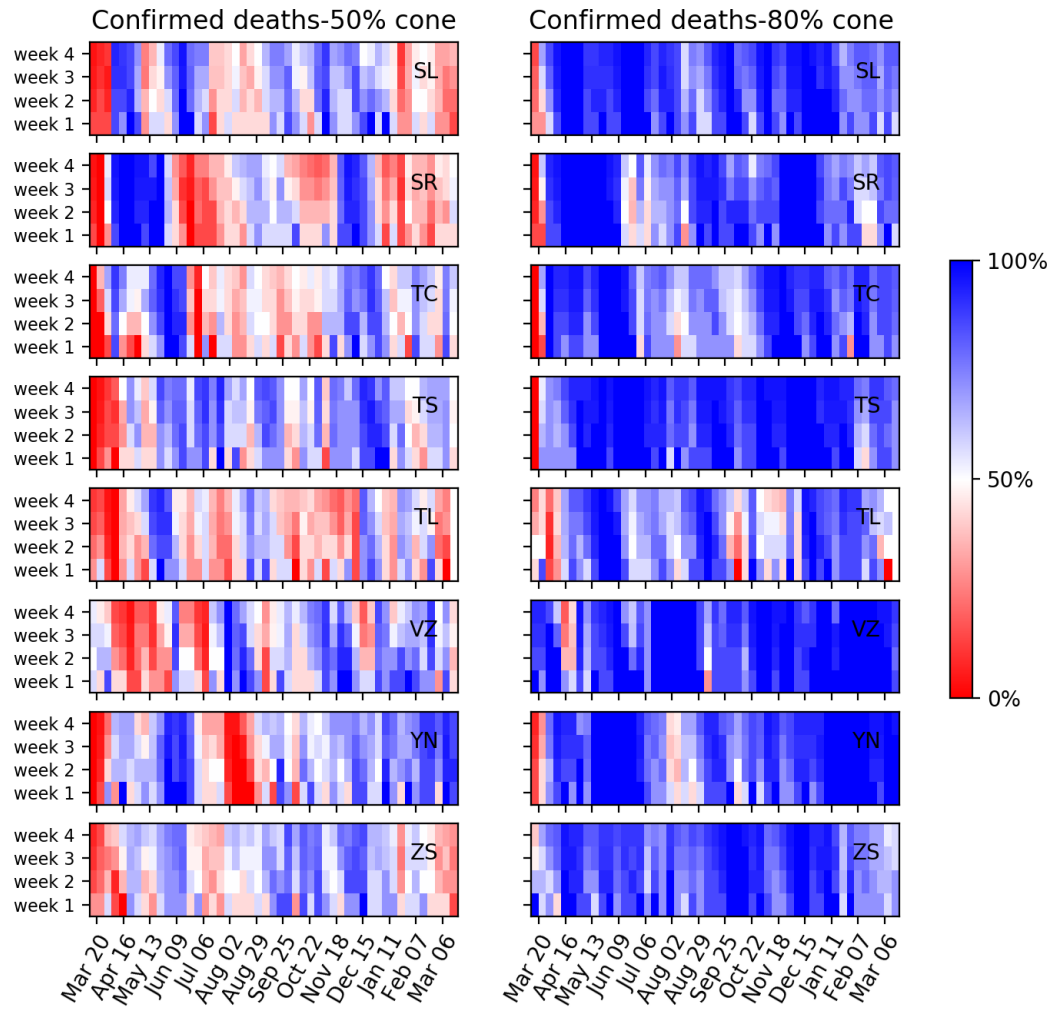


Figure S19: **Heatmap of the one to four week forecasts' performance of confirmed deaths**, see Figure S16 for details.